Ceramics International 52 (2026) 12313–12342

Contents lists available at ScienceDirect

Ceramics International

journal homepage: www.elsevier.com/locate/ceramint

Review article

Silk-fibroin scaffolds enriched with calcium-based fillers for bone regeneration: a systematic review

Biagio Matera [a,1], Giuseppe De Giorgio [b,1], Katia Rupel [c,*], Gianluca Turco [c], Pasquale D'Angelo [b,**], Benedetta Ghezzi [a,b,***]

[a] Centre of Dental Medicine, Department of Medicine and Surgery, University of Parma, Via Gramsci 14, 43126, Parma, Italy
[b] IMEM-CNR, Parco Area delle Scienze 37/A, 43124, Parma, Italy
[c] Department of Surgical, Medical and Health Sciences, University of Trieste, Piazza Dell'Ospitale 1, 34129, Trieste, Italy

ARTICLE INFO

Keywords:
Silk fibroin
Calcium-based fillers
bone regeneration
3D scaffolds
Biomaterials

ABSTRACT

Bone regeneration remains a major challenge in modern medicine. Silk Fibroin (SF), a natural biopolymer derived from Bombyx mori is gaining an increasing attention due to its remarkable biological properties. The combination of SF with calcium-based (CaP) fillers such as hydroxyapatite (HAp),F062-tricalcium phosphate (F062-TCP), octacalcium phosphate (OCP), amorphous calcium phosphate (ACP), and others, allows the production of 3D composite scaffolds with enhanced osteogenic properties.

This systematic review aims to critically evaluate the current literature on the use of SF-based 3D scaffolds implemented with calcim-based fillers for bone tissue engineering.

A comprehensive search of PubMed, Science Direct and Scopus databases has been conducted according to PRISMA guidelines. Preclinical in vitro and in vivo results published in the last decade were included and data concerning scaffold fabrication methods, composition, structural and mechanical properties, in vitro and in vivo regenerative outcomes were extracted.

A total of 19 studies met the inclusion criteria. Most scaffolds were fabricated via freeze-drying, salt-leaching, lyophilisation and electrospinning techniques, alone or combined. In the majority of cases, the incorporation of CaP-based fillers significantly improved scaffold bioactivity, mechanical strength, hence promoting osteoblasts proliferation and differentiation in vitro, while in vivo models demonstrated an enhanced bone formation.

SF-based scaffolds enriched with CaP fillers may therefore represent a concrete and valuable solution for the treatment of critical sized bone defects, allowing the overcoming of clinical limitations linked to the classic surgical treatments. However, further studies and clinical trials are essential to validate and translate these results in humans.

Key points

-Silk fibroin (SF) and inorganic fillers boost scaffold bioactivity, and osteogenic potential
-Scaffold fabrication methods affect porosity, structure, and biological performance
-SF scaffolds/CaP-based fillers enhance bone formation, and mineral density *in vivo* models
-nHAp and HAp is the most employed filler for SF-based scaffolds
-Freeze-drying is the most employed technique to create SF-based scaffolds

1. Introduction

The treatment of bone defects represent a significant challenge for the modern medicine, especially due to the complex nature of the bone

* Corresponding author. Department of Surgical, Medical and Health Sciences, University of Trieste, Piazza Dell'Ospitale 1, 34149, Trieste, Italy.
** Corresponding author. IMEM-CNR, Parco Area delle Scienze 37/A, 43124, Parma, Italy.
*** Corresponding author. Dept. of Medicine and Surgery, Via Gramsci 14/A, 43126, Parma, Italy.
E-mail addresses: biagio.matera@unipr.it (B. Matera), giuseppe.degiorgio@imem.cnr.it (G. De Giorgio), krupel@units.it (K. Rupel), gturco@units.it (G. Turco), pasquale.dangelo@imem.cnr.it (P. D'Angelo), benedetta.ghezzi@unipr.it (B. Ghezzi).
[1] These authors contributed equally to this work.

https://doi.org/10.1016/j.ceramint.2026.01.443
Received 20 October 2025; Received in revised form 9 January 2026; Accepted 27 January 2026
Available online 31 January 2026

tissue which is a highly vascularized and dynamic tissue with intrinsic but limited capacity for regeneration [1,2]. In fact, in cases of skeletal anomalies that can result from acute and chronic diseases, age-related bone loss or traumatic accidents, bone grafting surgery and tissue engineering are needed to promote bone regeneration [3]. Approximately 2 millions of bone grafting procedures are performed every year, with an estimated annual growth rate of 13% [4,5]. In the field of dentistry, the use of bone grafts and substitutes have markedly increased in recent years due to advancements in dental implantology and the growing need for repair of craniofacial bony defects, although still having several limitations and >50% of failure rate [6–8].

Advances in tissue engineering have led to the development of various materials and techniques for bone regeneration, taking into account that the ideal material to replace bone tissue should meet precise specifications, such as biocompatibility, biodegradability, osteoconductivity, osteoinductivity, having appropriate mechanical characteristics, porosity, safety, and cost-effectiveness [9]. Bone autografts remain the gold standard for bone repair. It includes all three crucial components for tissue regeneration: an osteoconductive scaffold, osteoinductive signaling molecules, and osteogenic cells. However, autografts are limited in availability, and harvesting bone can lead to pain and complications at the donor site [10]. These limitations foster the development of novel synthetic or natural materials to be used as grafts for bone replacement and regeneration.

Among bone substitutes, bioactive three-dimensional (3D) scaffolds may take advantage from highly porous and interconnected structures that can be colonized by cells via adequate processing routes of (bio) materials, whose choice is crucial to confer adequate mechanical properties to the structures [11]. Many natural and synthetic biomaterials, mainly polymers (*e.g.* chitosan, alginate, etc.), have been used to develop bone constructs able to support bone tissue engineering (BTE) [12–16].

Silk fibroin (SF), a natural macromolecular protein mainly derived from silkworms, has been increasingly explored as a biomaterial for applications in tissue engineering and regenerative medicine due to its ease of manufacturing, biocompatibility and biodegradability [17,18].

Although SF–based scaffolds are widely employed in BTE due to SF biocompatibility, their use as standalone materials is still limited by not completely adequate mechanical strength, as well as suboptimal osteoinductive and osteoconductive properties [19–22]. To overcome these limitations, the integration of calcium-based materials able to enhance mechanical strength and to define the surface topography by mimicking the one of the native bone structure, represents a robust strategy pursued by dedicated research. In particular, β -tricalcium phosphate (β-TCP) or hydroxyapatite (HAp), the main inorganic component of bone, represents widely researched bone substitutes able to offer strong osteoconductive properties and to guarantee adequate support to bone regeneration [3,23,24]. Indeed, SF implemented with Calcium/HAp shows extraordinary properties for bone repair, as its fibrous structure resembles the collagen I fibers disposition and, at the same time, its β-sheets can both act as nucleation site for the deposition of nanocrystals, thus influencing its degradation time [25]. Related SF-based scaffolds show high biocompatibility, high processability, degradation, flexibility, outstanding mechanical properties, and low immunogenicity [26]. For these reasons, they have been widely used in many regenerative areas, *e.g.* for the reconstruction of cartilage tissue, ligaments, tendons, skin, wounds, tympanic membranes and also in guided bone regeneration (GBR) [27]. Furthermore, SF-based scaffolds, by mimicking the composition of extracellular matrix, offer a suitable physical framework that facilitates interaction with cells and blood vessels. Upon implantation, this structure supports tissue regeneration by enabling cellular and vascular infiltration into the scaffold's pores, thereby promoting subsequent cell proliferation. As granulation tissue forms, the scaffold gradually degrades and is fully replaced by the target tissue [28].

The scaffold morphology and structure largely influence clinical applicability and, as stated above, they are determined by the production methods. Different components, parameters, and post-treatment methods were described to modify the pore size, and porosity and the most frequently used techniques include electrospinning, freeze-drying, solvent casting, gas foaming, particulate leaching, and 3D printing [28].

Within the depicted scenario, this systematic review of the literature aims to describe the critical factors involved in designing and producing SF-based 3D scaffolds enriched with calcium/HAp for bone regeneration in the context of both orthopedic and maxillofacial/dental applications. Particular attention will be paid to the following aspects.

1. chemical properties of scaffolds, including the production methods
2. structural and morphological characteristics, with particular insight on the mechanical testing
3. *In vitro* and *in vivo* testing procedures, including results of cell proliferation/osteogenic differentiation assays and 3D graft osteointegration, respectively.

2. Materials and methods

The primary objective of this systematic review is to evaluate the role of various types and concentration ratios among calcium-based components integrated within SF matrices, focusing on osteoblastic behavior in terms of proliferation and differentiation (for *in vitro* studies), and on the impact of these materials on bone regeneration parameters, such as new bone formation, bone volume fraction (BV/TV), and bone mineral density, upon *in vivo* analysis. Moreover, production methods of the synthetic bone grafts have been investigated to evaluate their influence on mechanical and morphological properties of the 3D structures.

The search strategy included, prior to the selection process, the election of two different queries for electronic search on PubMed, Science Direct and Scopus, as reported in Table 1.

A two-stage screening has been performed by two independent reviewers, firstly browsing title and abstract, and then reading the full text of works identified basing on the selected inclusion and exclusion parameters. The screening process has been initially calibrated by the selection of 100 papers to ensure uniformity of selection criteria while implementing this procedure. Studies with insufficient information in the title or abstract to allow a clear decision, as well as studies with reviewer disagreements, were advanced to the next screening stage. During the second-stage screening (full-text analysis), disagreements

Table 1
Search strategies applied for electronic search on PubMed, Science Direct and Scopus databases.

Database	Search Query
PubMed	(Silk fibroin) OR (silk)) OR (fibroin)) AND (Calcium phosphate)) OR (TCP)) OR (BTCP))) OR (b-TCP)) OR (beta-TCP)) OR (HAp)) OR (HA)) OR (hydroxyapatite)) AND (bone regeneration)) OR (bone)) OR (bone graft)) OR (bone substitute)) OR (bone replacement)) AND (scaffold)) OR (3D scaffold)) NOT (cartilage)) NOT (vascular)) NOT (nerve)) NOT (review)) NOT (meta-analysis)) NOT (systematic review)) NOT (hyaluronic acid) AND (y_10[Filter]) AND ((y_10 [Filter]) AND (medline[Filter]) AND (english[Filter]))) NOT (editorial) AND ((y_10[Filter]) AND (medline[Filter]) AND (english [Filter]))) NOT (PLA)) NOT (PLGA)) NOT (PLLA)) NOT (collagen) AND ((y_10[Filter]) AND (medline[Filter]) AND (english[Filter]))) AND ((y_10[Filter]) AND (medline[Filter]) AND (english[Filter])) AND ((y_10[Filter]) AND (medline[Filter]) AND (english[Filter]))) NOT (nanoparticles)) NOT (nanowires)) NOT (skin)) NOT (pancreas)) NOT (eye)) NOT (cardiac)) NOT (heart)) NOT (neural)) NOT (ligament)) NOT (spinal cord)) NOT (inter-vertebral)) NOT (bladder)) NOT (tracheal)
Science Direct	Silk fibroin AND Calcium OR hydroxyapatite AND bone regeneration OR bone graft AND 3D scaffold NOT gelatin NOT cartilage NOT vascular
Scopus	Silk fibroin AND Calcium OR hydroxyapatite AND bone regeneration OR bone graft AND 3D scaffold NOT gelatin NOT cartilage NOT vascular

between the two reviewers were resolved through discussion with a third reviewer.

To ensure the inclusion of both published and unpublished data, a manual search focused on works published in the previous two years was performed in high-impact journals (Journal Citation Report™, Clarivate) with a high publication rate on this topic (*e.g.* Bioactive materials, Biomaterials and Biomaterials research).

Additionally, the reference lists of the selected papers were manually reviewed to identify studies that met the specified inclusion criteria.

2.1. Eligibility criteria

2.1.1. Type of studies

This systematic review includes original research papers written in english and published between 2014 and 2025 that analyze *in vitro* and *in vivo* studies employing SF structures loaded with calcium-based materials (*e.g.* HAp, β-TCP, octacalcium phosphate (OCP), etc.) for bone regenerative applications.

Systematic and narrative reviews, meta-analysis, book chapters, conference papers, conference proceedings, and editorials as well studies unrelated to SF scaffolds loaded with calcium-based materials have been excluded. Absence of a control group using unloaded SF scaffolds and applications outside the field of bone regeneration have also been considered as exclusion criteria.

2.2. Participants

In vitro studies: papers investigating 3D scaffolds enriched with calcium-based materials and tested with various cell type (*e.g.* BMSCs, hMSCs, MC3T3-E1, hACSs) to assess their response to SF and SF loaded with calcium-based materials.

In vivo studies: research involving any animal model, irrespective of sex, age, or species, and treated with SF 3D scaffolds enriched with calcium-based materials.

2.3. Intervention

The intervention was characterized by *in vitro* or *in vivo* studies with bioengineered three-dimensional SF-based scaffolds loaded with various types and concentrations of calcium-based fillers.

2.4. Comparison

In vitro or *in vivo* studies with three-dimensional SF-based scaffolds not loaded with other components.

2.5. Outcomes

For *in vitro* studies, production method, morphological and structural features of SF scaffolds (*i.e.* type and particle size of filling material, presence of additional components, porosity, pore size, compressive modulus, compressive strength, water uptake, swelling ratio and scaffold degradation) have been evaluated, as well as the biological response has been investigated in terms of cellular proliferation and differentiation.

On the counterpart, for *in vivo* studies, the biological response to the insertion of the biomaterial has been quantified in terms bone formation, percentage of bone volume/total volume and bone mineral density.

2.6. Data extraction and analysis

This systematic review extracted and analyzed data related to scaffold structural, *in vitro*, and *in vivo* properties to comprehensively assess the performance of SF-based composite scaffolds loaded with CaP-based fillers.

Data extraction was performed independently by two reviewers; in cases of missing or ambiguous information, the corresponding authors of the included studies were contacted via email to request clarification. In case of non-response all the results have been extracted through Plot Digitizer (https://plotdigitizer.com/), a software employed to digitize scanned plots of functional data approved by Cochrane [29].

Relevant data were extracted from the included studies using specific data extraction tables structured according to the following parameters to evaluate i) structural properties (*i.e.* scaffold porosity, pore size, compressive modulus/strength, water uptake, scaffold degradation, etc), ii) *in vitro* and iii) *in vivo* outcomes.

Specifically, for structural characterization, the collected data included study details (*e.g.* authors, publication year, country, study setting, funding) and scaffold features (*e.g.* scaffold structural morphology, type of fibroin employed, calcium-based components and their concentration, particle size, additional compounds, and fabrication method). The main structural outcomes were analyzed in terms of porosity, pore size, compressive modulus, compressive strength, water uptake, swelling ratio, and degradation rate.

In vitro analyses focused on experimental conditions (cell type, *in vitro* assays, experimental time points, control and intervention details) and reported primary outcomes such as proliferation and osteogenic differentiation. *In vivo* studies included data on experimental design (control/intervention groups, animal model employed, number of animals, defect type, follow-up duration) and the evaluation of bone regeneration by measuring new bone formation, bone volume fraction (BV/TV), and bone mineral density (BMD). This combined approach allowed for a multiparametric comparison of scaffold performance across biological, mechanical, and regenerative parameters.

3. Results

The search strategy was performed on three main databases (PubMed, Scvience Direct and Scopus) on the February 22, 2024 and search was updated on July 18, 2025, allowing the identification of a total of 14933 records from three different databases, as detailed in Fig. 1.

Moreover, 19 additional records have been identified through manual search. After duplicates removal, 8624 records have been screened based on title and abstract and 8580 papers have been excluded as they did not match the inclusion criteria. From the remaining 44 records, 25 papers have been excluded after full-text analysis; reasons for exclusion are detailed in Table 1S of the supplementary information. Nineteen articles were included in the final analysis. Records identification, screening, eligibility and inclusion process are reported in Fig. 1.

Among the selected studies, about 42% of papers were related to *in vitro* applications of the 3D composite structures [23,30–36], about 5% for *in vivo* [37], and about 53% of studies were related to *in vitro* and *in vivo* applications [38–47]. Studies setting, along with the composition of the tested biomaterials are detailed in Table 2.

3.1. Fabrication and morphological/mechanical properties of calcium-derived composite loaded SF scaffolds

Detailes about fabrication techniques as well as the specific SF scaffolds components used to create the calcium-based biomaterials included in this systematic review, and the typologies of obtained scaffolds are summarized in Fig. 2.

3.2. Composition of SF scaffolds

All the studies included in this systematic review adopted an aqueous SF solution as principal component for the scaffolds fabrication, except for Park et al. that employed properly processed woven SF sutures [37]. The SF aqueous solutions in all cases were obtained by canonical SF processing protocols using LiBr [48] or Aijisawa reagent as dissolving

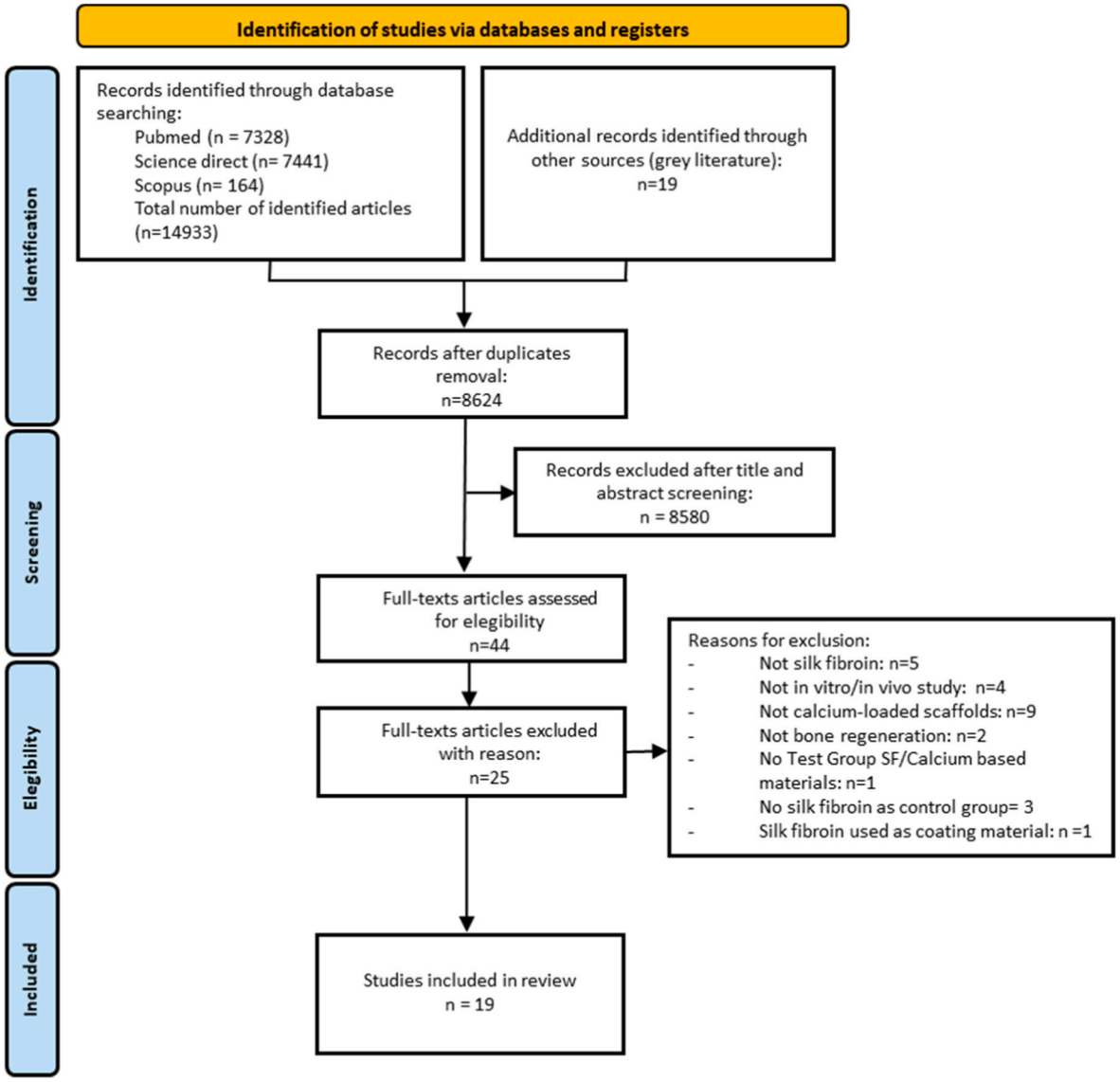

Fig. 1. PRISMA flow diagram illustrating the study selection process. The diagram shows the number of records identified, screened, assessed for eligibility, and included in the review, along with reasons for exclusions.

agents, followed by dialysis to remove salts [49]. In one study, Zhu et al. further processed the aqueous SF by adding NaClO solution in an alkaline environment [40]. This step introduced additional carboxyl groups and enhanced the electronegativity, theoretically providing additional sites for successive mineralization.

Another key factor herein considered and analyzed was the type of calcium-based composite utilized for the fabrication of SF-based scaffolds; Table 2 reports the different calcium formulations amounts employed and relative particle size when reported. In the 32% of the studies, nHAp was used). Different methods of nHAp load up were employed [34,36–39,41]. Park et al. utilized nHAp as coating of SF woven sutures, while in Liu et al. samples nHAp was assembled into SF scaffolds by a modified two-step mineralization process [37,39].

Kim et al. and Yu et al. dispersed HAp nanoparticles directly into the SF aqueous solution during the material synthesis, also Shao et al. dispersed the HA nanoformulation into the SF solution prior to the material synthesis process [34,36,41]. Lastly, Tang et al. added nHAp to the Hexafluoroisopropanol (HFIP) solvent to create a composite solution with SF to prepare electrospun nanofiber scaffolds [38]. Another largely employed calcium-derived compound was β-TCP, which use has been detected in five different studies, and in all cases β-TCP powders were dispersed into aqueous SF solutions [23,30,42–44]. Five studies related to the dispersion of HA into the structural material [31,33,35,46,47]. However, it is important to highlight the approach in which HA was functionalized with with Glycidoxypropyltrimethoxysilane (GPTMS) to enhance its dispersion within the SF matrix [46]. Also, in the work from Lyu et al. HA coatings were synthesized by depositing supersaturated ions from a mineralized solution, thus in this case HA results to not be interspersed into the material [47]. In one work calcium phosphate (CaP) was employed and calcium chloride and ammonia dibasic phosphate were introduced into an aqueous SF solution to generate a suspension that further mineralized, forming HA embedded into the final scaffold [32]. CaP, in an amorphous conformation, was employed by Zhu et al. via a mixture of poly-aspartic acid sodium, $CaCl_2$ and Na_2HPO_4 added in powder dispersion to SF solution and allowed to generate ACP during the material synthesis process [40]. Finally, in OCP was loaded into the scaffolds by a heterogeneous precipitation method. Briefly, to obtain a SF-OCP composite precipitation was exploited the co-precipitation between SF solution with calcium acetate and sodium dihydrogen phosphate acting as OCP precursors [45].

Some studies included additional non-biological components to enhance scaffolds properties (Table 2). Kim et al. blended

Table 2
Detailed summary of the scaffold compositions and fabrication techniques described in the systematic review.

First Author and Year	Country and Study Setting	Type of scaffolds	Type of Fibroin	Calcium-based components; relative amount; particle size	Additional components		Production method	Test groups (*in vitro/in vivo*)				
					Non Biological	Biological		Control Group	Intervention Group 1	Intervention Group 2	Intervention Group 3	Intervention Group 4
Han F. et al., 2019 [45]	China, University and Private Research Institutes	3D porous scaffold	SF	OCP; 40 mM of calcium acetate and sodium dihydrogen phosphate; OCP: 489 ± 399.1 nm; 0.1SF-OCP: 102.2 ± 50.7 nm; 0.3SF-OCP: 94.7 ± 48.4 nm; 1SF-OCP: 223.7 ± 167.6 nm	None	None	Freeze-drying	SF	SF/OCP	N.A.	N.A.	N.A.
Huang X. et al., 2015 [33]	China, University	3D porous scaffold	SF	HAp; 20% irregular HAp aggregates (SF-A20HA) 20% HAp/silk core–shell NPs (SF-D20HA), 40% irregular HAp aggregates (SF-A40HA) 40% HAp/silk core–shell NPs(SF-D40HA); Length: 150–200 nm Width: about 65 nm	N.A	N.A.	Freezing at −20 °C overnight to solidify the solvent, and then lyophilization.	SF	SF-A20HA	SF-D20HA	SF-A40HA	SF-D40HA
Jing T. et al., 2022 [44]	China, University	3D porous scaffold	SF	β -TCP SF/β -TCP ratio 2:1, 1:1, 1:2 1g; 0.5g; 0.25g, respectively; 400–600 nm	None	None	Freezing and lyophilization followed by EDC/NHS crosslinking	SF	SF/β -TCP 2:1 (2/1)	SF/β -TCP 1:1 (1/1)	SF/β -TCP 1:2 (1/2)	N.A.
Kim J. et al., 2016 [31]	South Korea, University	3D porous scaffold	SF	HAp; 10%w/v HAp; N.A.	TiO_2	N.A.	Sol-gel synthesis for TiO_2 NPs. SF 3D scaffolds salt leaching and stabilization at 60 °C followed by drying in desiccator	SF	SF/HA	SF/TiO_2/HA	N.A.	N.A.
Kim M. et al., 2017 [36]	South Korea, University, Private Research Institutes and Company	3D porous scaffold	SF	nHAp; 0–3% wt; <200 nm	PVP (1% wt)	None	Lyophilized SF/nHAp composite hydrogels	SF	SF-1% HAP	SF-2% HAP	SF-3% HAP	N.A.
Ko E. et al., 2018 [46]	Korea, University and Private Research Institutes	Electrospun 3D Nanofibrous Scaffold	SF	HAp; 20% w/w; <200 nm	PDA	N.A.	Electrospinning followed by freeze-drying followed by a second PDA coating stage.	SF	SF/HAp	HAp-PDA-SF/HAp	N.A.	N.A.

(*continued on next page*)

Table 2 (*continued*)

First Author and Year	Country and Study Setting	Type of scaffolds	Type of Fibroin	Calcium-based components; relative amount; particle size	Additional components		Production method	Test groups (*in vitro/in vivo*)				
					Non Biological	Biological		Control Group	Intervention Group 1	Intervention Group 2	Intervention Group 3	Intervention Group 4
Lee D.H. et al., 2017 [42]	Republic of Korea, Private Research Center	3D porous scaffold	SF	β -TCP; SF100: 0 wt% β -TCP; SF75/β -TCP25: 25 wt β -TCP%; SF50/β -TCP50: 50 wt% β -TCP; SF25/β -TCP75: 75 wt% β -TCP; N.A.	None	None	FreezIng and lyophilization	SF	SF75/β -TCP25	SF50/β -TCP50	SF25/β -TCP75	N.A.
Liu F. et al., 2020 [23]	China, University	3D porous scaffold	SF	β -TCP; β -TCP:GO:SF/SPI 10 mg:10 mg:10 mL; N.A.	SPI and GO NPs	N.A.	Freeze-drying and additional crosslinking step with EDC/ NHS	SF	SF/SPI/β -TCP	SF/SPI/β -TCP/GO	N.A.	N.A.
Liu H. et al., 2015 [39]	China, University and Private Research Institutes	3D porous scaffold	SF	nHAp; N.A.; N.A.	None	None	Salt leaching and freeze-drying followed by two-step mineralization	SF	SF-nHAp	N.A.	N.A.	N.A.
Lyu R. et al., 2025 [47]	China, University	3D composite membrane	SF	nHAp; N.A. N.A.	Zn^{2+}, Mg^{2+}	N.A.	SF membranes have been fabricated by drip-dry method. Electrochemical deposition has been employed to cover the surface with HAp formed by the deposition of Ca^{2+}, Zn^{2+}, Mg^{2+} and PO_4^{3-} layer by layer	SF	SF/H	N.A.	N.A.	N.A.
Park J.Y. et al., 2015 [37]	South Korea, University	3D porous scaffold	SF	nHAp (coating); 0.15g; N.A.	None	DPCS and PDLCs	Scaffolds constructed using a weaving machine, then degummed and loaded with nHAp. Finally soaked in Collagen solution and freeze dried	SF	PDLC-silk scaffold (PDLSS)	DPC-silk scaffold (DPSS)	N.A.	N.A.
Park H.J. et al., 2016 [43]	Korea, University and Private Research Institutes	3D porous scaffold	SF	β -TCP; SF/β -TCP 1:1; 300–600 μm for small granules size (GS); 600–1000 μm for medium granules size (GM)	None	None	Freeze-drying	SF	GS	GM	N.A.	N.A.
Pina S. et al., 2017 [30]	Portugal, University and Hospital	3D porous scaffold	SF	β -TCP; 30% w/w; N.A.	$(Ca[NO_3]_2 \cdot 4H_2O)$; $([NH_4]_2 \cdot HPO_4)$; $(Sr[NO_3])$; $(Zn[NO_3])$; $(Mn[NO_3]_2 \cdot 4H_2O)$	None	Salt leaching, solidification at room temperature and lyophilization	SF	SF/β -TCP	N.A	N.A	N.A
Shahid A. et al.,	Pakistan, University	3D porous scaffold	SF	HAp; 40 wt% (320 mg); N.A.	SA and Mg–ZnO	N.A.	Freeze gelation and drying in oven for 72 h followed by	SF	SF/H	N.A	N.A	N.A

(*continued on next page*)

Table 2 (*continued*)

First Author and Year	Country and Study Setting	Type of scaffolds	Type of Fibroin	Calcium-based components; relative amount; particle size	Additional components		Production method	Test groups (*in vitro/in vivo*)				
					Non Biological	Biological		Control Group	Intervention Group 1	Intervention Group 2	Intervention Group 3	Intervention Group 4
2024 [35]							vacuum drying for 72 h, both at 37 °C.					
Shao Y. F. et al., 2024 [34]	China, University	3D porous scaffolds	SF	nHAp; 10% v/v lenght: 126 ± 21 nm width: 23 ± 3 nm	N.A.	N.A.	10 wt % HAp powder dispersed in 10% v/v 1-butyl alcohol via ultrasound, then added dropwise to SF. Freeze-drying process has been followed.	b-SF	b-HA/SF	N.A	N.A	N.A
Tang Z. et al., 2024 [38]	China, University and Hospital	Electrospun 3D Nanofibrous Scaffold	SF	nHAp; SF:PCL:HA (5:5:1); N.A.	Se NPs	N.A.	Electrospinning of composite and transformation of the nanofiber mixed dispersions into aerogel, then scaffolds are obtained by hot pressing eliminating the need for cross-linking agents	SF	HA	N.A.	N.A.	N.A.
Yan L.P. et al., 2014 [32]	Portugal, University and Private Research Institutes	3D porous scaffold	SF	CaP; 16 wt%; N.A.	N.A.	N.A.	Salt-leaching air drying solidification, followed by freeze-drying	S16	SC16	N.A.	N.A.	N.A.
Yu X. et al., 2021 [41]	China, University	3D porous scaffold	SF	nHAp; 200 mg; Length: 100–300 nm Width: 20–30 nm	N.A.	Naringin; Gelatin Micro-spheres	Lyophilization at −60 °C followed by EDC-NHS crosslinking and secondary lyophilization	SF	nHA/SF	N.A.	N.A.	N.A.
Zhu Y. et al., 2024 [40]	China, University and Private Research Institutes	Injectable hydrogel	OxSF	ACP; N.A.; N.A.	None	PRP	Hydrogel obtained by extrusion. Sonication was used to trigger the solidification and polymerization of the SF and OxSF network.	SF	OxSF	OxSF/ACP	OxSF/ACP/ PRP	N.A.

Abbreviations employed: Silk Fibroin (SF); Octacalcium Phosphate (OCP); Nanoparticles (NPs); β -Tricalcium Phosphate (β-TCP); Hydroxyapatite (HAp); Nano-hydroxyapatite (nHAp); Poly(vinylpyrrolidone) (PVP); Polydopamine (PDA); Soy Protein Isolate (SPI); Graphene Oxide (GO); Primary Dental Pulp Cells (DPCs); Periodontal Ligament Cells (PDLCs); Calcium nitrate tetrahydrate (($Ca[NO_3]_2 \cdot 4H_2O$)); diammonium hydrogen phosphate (($[NH_4]_2 \cdot HPO_4$)); strontium nitrate (($Sr[NO_3]$)); zinc nitrate (($Zn[NO_3]$)); manganese (II) nitrate tetrahydrate (($Mn[NO_3]_2 \cdot 4H_2O$)); Succinic Acid (SA); Magnesium doped zinc oxide (Mg-ZnO); Poly-ε-caprolactone (PCL); Selenium (Se); Calcium Phosphate (CaP); Oxidized silk fibroin (OxSF); Amorphous Calcium Phosphate (ACP); Platelet-Rich-Plasma (PRP); Not applicable (N.A.).

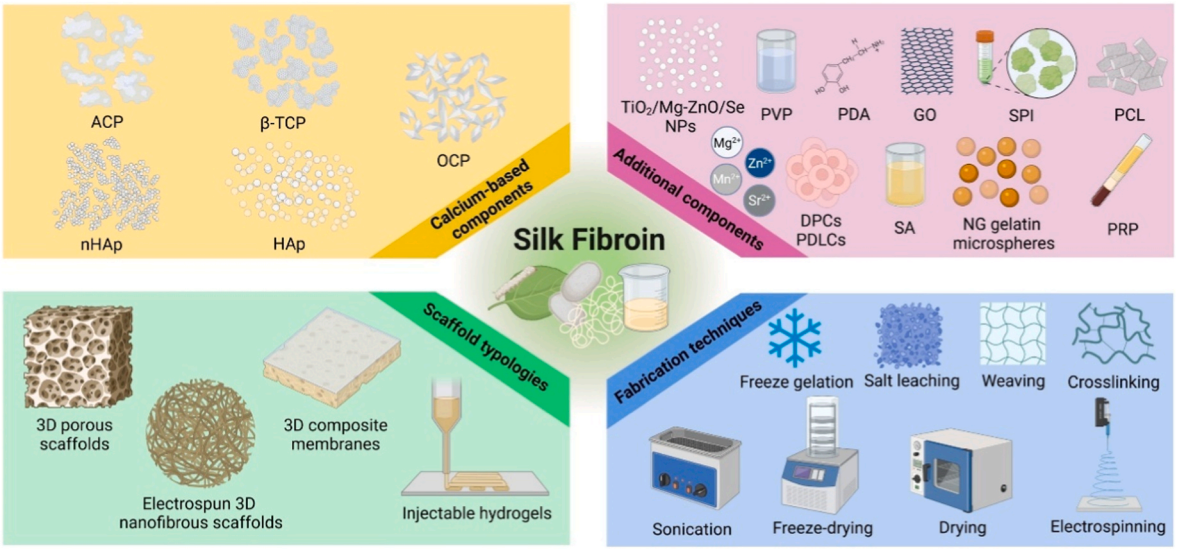

Fig. 2. Detailed scheme of SF scaffolds components, additional components, fabrication techniques and scaffolds typologies obtained from the studies included in the systematic review. Abbreviations employed: Silk Fibroin (SF); Octacalcium Phosphate (OCP); β -Tricalcium Phosphate (β-TCP); Hydroxyapatite (HAp); Nano-hydroxyapatite (nHAp); Amorphous Calcium Phosphate (ACP); Titanium dioxide nanoparticles (TiO_2 NPs); Magnesium-doped zinc oxide nanoparticles (Mg-ZnO NPs); Selenium nanoparticles (Se NPs); Poly(vinylpyrrolidone) (PVP); Polydopamine (PDA); Graphene Oxide (GO); Soy Protein Isolate (SPI); Poly-ε-caprolactone (PCL); Primary Dental Pulp Cells (DPCs); Periodontal Ligament Cells (PDLCs); Succinic Acid (SA); Naringin gelatin microspheres (NG gelatin microshperes); Platelet-Rich-Plasma (PRP). Created in https://BioRender.com.

polyvinylpyrrolidone (PVP) to SF and nHAp dispersion to improve nanoparticles homogeneous distribution [36]. In Pina's work, SF based scaffold were doped by adding Sr, Zn, and Mn, ionic doping increased degradation behavior and compressive mechanical strength [30]. Ionic doping represents a common strategy to enhance several scaffold's properties, SF/HAp composite membranes were mineralized with Zn^{2+} or Mg^{2+} combinations enhanced physiological functions and promoted osteogenic markers and gene expression, with Zn showing superior collagen deposition [47]. Another study by Kim et al., showed the possibility to add TiO_2 nanoparticles into the SF and HA solution prior to the scaffold's synthesis process, leading to increased mechanical properties and higher porosity [31]. Similarly, also the incorporation into SF scaffolds of soy protein isolate (SPI) and graphene oxide (GO) nanoparticles, and β-TCP, showed increased compressive strength. Specifically, GO enhanced water adsorption and porosity providing additive functional groups for cellular mineralization by increasing the surface/volume ratio, and consequently cell adhesion [23]. Ko et al. operated an additional functionalization to SF and SF/HA scaffolds; in this case the adhesive properties of polydopamine (PDA) were exploited by treating the materials with dopamine solution in an alkaline environment, allowing the formation of an adhesive layer. A secondary HA deposition over the PDA layer greatly increased mechanical properties and osteogenic efficacy of HAp/PDA/SF scaffolds [46]. Finally, Selenium nanoparticles (SeNPs) were added to electrospun SF/polycaprolactone (PCL) nanofibers, subsequently hot pressed to fabricate SF/PCL/nHA/Se scaffolds [44]. This process generated an external layer characterized by a compact structure, where Se nanoparticles were uniformly distributed. Conversely, the innner layer had a loose and porous structure helpful for cell adhesion. This formulation also proved excellent behavior in mechanical tests, with a tensile strength of 4.15 MPa, accompanied by good flexibility [38].

Only in about the 16% of the cases, also biological components were utilized as additives to tune the final material properties or to boost the interaction within biological environments. Park et al. directly seeded cells onto the silk scaffolds; dental pulp and periodontal ligament cells that were extracted from human prior to *in vivo* experiments, showing attachment of the cells onto SF and production of extracellular matrix [37]. In the second study platelet-rich plasma (PRP) was collected, mixed with OxSF and ACP, and processed to generate a composite hydrogel. The integration of PRP significantly reduced the gelation time, enhancing at the same time compressive stress and mineralization performances compared to the other groups [40]. In the third case Yu et al. loaded naringin (NG), a naturally derived polymethoxylated flavonoid, into gelatin microspheres (GM). NG loaded microspheres were dispersed into an nHAp/SF solution, and combined scaffolds were fabricated. NG/nHAp/SF scaffolds exhibited superior mechanical characteristics in comparison to other experimental groups with higher osteoinductivity and osteogenic potential [41]. A complete overview of the described characterstics is stated in the following table.

3.3. Scaffolds fabrication techniques

Another main aspect herein examined was the scaffolds production technique (Fig. 2). 8 out 19 studies utilized lyophilization (also named freeze-drying by some authors) as principal fabrication technique of SF materials [23,33,36,41–45]. Kim et al. prior to lyophilization, treated the SF composite solution by a γ-ray irradiation process to trigger a hydrogel formation. In four studies lyophilization was followed by additional treatments [36]; in Jing et al. and Liu et al. works, dried scaffolds were processed with EDC (1-ethyl-3-(3-dimethylaminopropyl) carbodiimide) and NHS (N-hydroxysuccinimide) acting as crosslinker agents to further strengthen the as-prepared materials [23,44]. Huang et al. produced SF/HAp composite porous scaffolds by freezing the compound at −20 °C overnight to solidify the solvent prior to a lyophilization step and subsequent crystallization of the scaffolds in 80% (v/v) methanol [33]. Lastly, Han et al. employed an ethanol treatment was exploited to enhance SF crystallization degree and material's mechanical properties [45]. It is important to point out that, in almost all studies, the use of lyophilization was often found in combination with a production technique, hence acting as post-processing step to dry up the scaffolds. Similarly, in Shahid et al.'s project, scaffolds were prepared using the freeze gelation method by pouring the SF-based solutions into molds and freezing at −20 °C for 12 h, then to −40 °C for an additional 24 h. After the initial 12 h freezing period, precooled absolute ethanol was added in three steps to the frozen and gelate the scaffolds, after this process scaffolds were dried in a drying oven for 72 h followed by vacuum

Table 3
Overview of scaffold composition, structural characteristics, and performance parameters reported across studies included in the systematic review. Data include porosity (%), pore size (μm), compressive modulus, compressive strength, water uptake, swelling ratio, and scaffold degradation for both control and intervention groups. Abbreviations employed: Silk Fibroin (SF); Octacalcium Phosphate (OCP); β -Tricalcium Phosphate (β-TCP); Hydroxyapatite (HA or HAp or HAP); Nano-hydroxyapatite (nHAp); Soy Protein Isolate (SPI); Graphene Oxide (GO); Oxidized silk fibroin (OxSF); Amorphous Calcium Phosphate (ACP); Small Granules Size (GS); Medium Granules Size (GM); Not applicable (N.A.).

First Author and Year	Porosity		Pore size		Compressive modulus		Compressive Strength		Water Uptake (%)		Swelling Ratio (%)		Scaffold Degradation (%)	
	Control Group	Intervention Groups	Control Group	Intervention Groups	Control Group	Intervention Groups	Control Group	Intervention Groups	Control Group	Intervention Groups	Control Group	Intervention Groups	Control Group	Intervention Groups
Han F. et al., 2019 [45]	54.9%	SF/OCP 62.8%	41.2 ± 11.4 μm	SF/OCP: 111.9 ± 33.1 μm	N.A.	N.A.	N.A.	N.A.	N.A.	N.A.	N.A.	N.A.	N.A.	N.A.
Huang X. et al., 2015 [33]	N.A.	N.A.	N.A.	N.A.	89.37 ± 21.87 KPa	SF-A20HA:163.04 ± 33.98 KPa; SF-D20HA:245.31 ± 51.17 KPa; SF-A40HA:109.86 ± 40.23 KPa; SF-D40HA:547.07 ± 19.14 KPa	N.A.	N.A.	N.A.	N.A.	N.A.	N.A.	N.A.	N.A.
Jing T. et al., 2022 [44]	74.12 ± 2.18 %	SF/β -TCP 2:1 81.44 ± 7.74%; SF/β -TCP 1/1: 81.76 ± 8.15%; SF/β -TCP 1:2: 77.74% ± 6.58	128.42 ± 7.21 μm	SF/β -TCP 2:1133.45 ± 10.56 μm; SF/β -TCP 1:1: 212.88 ± 10.41 μm; SF/β -TCP 1:2: 202.63 ± 18.32 μm	N.A.	N.A.	0.32 ± 0.092 MPa	SF/β -TCP 2:1 0.51 ± 0.18 MPa; SF/β -TCP 1:1: 0.55 ± 0.08 MPa SF/β -TCP1:2: 1.11 ± 0.13 MPa	N.A.	N.A.	891.5	SF/β -TCP 2/1: 891.5 SF/β -TCP 1/1: 652.5 SF/β -TCP 1/2: 639.5	Week 1: 73.33; Week 8: 9.38	SF- βTCP (2/1) Week 1: 76.29; Week 8: 25.8; SF-βTCP (1/1) Week 1: 86.17; Week 8: 39.26; SF-βTCP (1/2) Week 1: 83.82; Week 8: 41.11;
Kim J. H. et al., 2015 [31]	65.11 ± 5.78 %.	SF/HA:70.60 ± 3.07 %; SF/TiO_2/HA: 72.39 ± 7.38 %	400–600 mm	400–600 mm	1.03 ± 0.01 MPa	SF/HA: 1.06 ± 0.11 MPa; SF/TiO2/HA: 1.36 ± 0.13 MPa	N.A.	N.A.	SF 82.75	SF/HA 39.03 SF/TiO2/HA 41.64	1000.6	SF/HA 351.9 SF/TiO_2/HA 362.5	N.A.	N.A.
Kim M. H. et al., 2017 [36]	81.8%	SF-1 (SF with 1% HAP) 87.3%; SF-2 (SF with 2% HAP) 86.8% SF-3 (SF with 3% HAP) 88.4%	130–250 μm (average pore size 161 ± 42 μm)	130–250 μm (average pore size 161 ± 42 μm)	N.A.	N.A.	7.5045 ± 2.160 kPa	SF-1:3.42 ± 0.29 kPa; SF-2:2.50 ± 0.29 kPa; SF-3:2.12 ± 0.42 kPa;	N.A.	N.A.	N.A.	N.A.	N.A.	N.A.
Ko E. et al., 2017 [46]	N.A.	N.A.	N.A.	N.A.	1.71 ± 0.93 kPa	SF/Hap: 3.43 ± 0.55 kPa; Hap-PDA-SF/Hap: 5.38 ± 0.96 kPa	N.A.	N.A.	N.A.	N.A.	N.A.	N.A.	N.A.	N.A.
Lee D. H. et al., 2017 [42]	74.12%	SF75/β -TCP25: 78.57%; SF50/β -TCP50: 80.57%;	140.7 μm	SF75/β -TCP25: 78.6 μm; SF50/β -TCP50: 130 μm; SF25/β	N.A.	N.A.	0.53 ± 0.63 MPa	(SF75/β -TCP25): 0.66 ± 0.15 MPa; (SF50/β -TCP50): 0.71 ± 0.08 MPa;	N.A.	N.A.	N.A.	N.A.	N.A.	N.A.

(*continued on next page*)

Table 3 (*continued*)

First Author and Year	Porosity		Pore size		Compressive modulus		Compressive Strength		Water Uptake (%)		Swelling Ratio (%)		Scaffold Degradation (%)	
	Control Group	Intervention Groups	Control Group	Intervention Groups	Control Group	Intervention Groups	Control Group	Intervention Groups	Control Group	Intervention Groups	Control Group	Intervention Groups	Control Group	Intervention Groups
		SF25/β -TCP75: 81.99%		-TCP75: 235.8 μm				(SF25/β -TCP75) 0.71 ± 0.07 MPa						
Liu F. et al., 2020 [23]	79.32 ± 1.62 %	SF/SPI/β -TCP:82.63 ± 1.04%; SF/SPI/β -TCP/GO: 80.45 ± 2.04%	117.76 ± 6.33 μm	SF/SPI/β -TCP: 232.53 ± 4.09 μm; SF/SPI/β -TCP/GO: 194 ± 6.18 μm	N.A.	N.A.	0.33 ± 0.09 MPa	SF/SPI/β -TCP: 1.02 ± 0.12 MPa; SF/SPI/β -TCP/GO: 0.80 ± 0.07 MPa	N.A.	N.A.	1661	SF/SPI/β -TCP: 1450; SF/SPI/β -TCP/GO: 1856	N.A.	N.A.
Liu H. et al., 2015 [50]	N.A.	N.A.	100–250 μm	100–250 μm	0.43 MPa	SF/nHAp: 1.52 MPa	N.A.	N.A.	N.A.	N.A.	N.A.	N.A.	N.A.	N.A.
Lyu R. et al., 2025 [47]	N.A.	N.A.	N.A.	N.A.	N.A.	N.A.	N.A.	N.A.	N.A.	N.A.	N.A.	N.A.	N.A.	N.A.
Park J. Y. et al., 2015 [37]	N.A.	N.A.	N.A.	20–80 μm	N.A.	N.A.	N.A.	N.A.	N.A.	N.A.	N.A.	N.A.	N.A.	N.A.
Park H. J. et al., 2016 [43]	60%	60% for both GS and GM	50 μm	50 μm for GS and GM	N.A.	N.A.	0.57 ± 0.01 MPa	GS: 0.71 MPa; GM: 0.72 MPa	95.88 ± 0.00	GS: 81.09 ± 1.37; GM:77.94 ± 1.87	17.43 ± 0.25	GS: 4.31 ± 0.37; GM 3.34 ± 0.36	N.A.	N.A.
Pina S. et al., 2017 [30]	64.7 ± 2.05	SF/β -TCP 39.6 ± 8.7	236.7 ± 9.9 μm	277.3 ± 43.8 μm	Dry state: 5.43 ± 0.53 MPa; wet state: 0.83 ± 0.12 MPa	Dry state: 15.16 ± 2.31 MPa; wet state: 2.76 ± 0.36 MPa	Dry state: 2.47 ± 0.36 MPa; wet state: 0.22 ± 0.04 MPa	Dry state: 4.36 ± 0.50 MPa; wet state: 0.60 ± 0.16 MPa	N.A.	N.A.	N.A.	N.A.	Day 30: 20%.	Day 30: 1–2%
Shahid A. et al., 2024 [35]	50 ± 3.31 %	SF/H 66.60 ± 3.65%.	N.A.	N.A.	N.A.	N.A.	N.A.	N.A.	N.A.	N.A.	Day 7: 0.17 ± 0.04 Day 14: 3.73 ± 0.19 Day 21: 6.67 ± 0.35 Day 28: 8.68 ± 0.46	SF/H Day 7: 7.34 ± 0.37 Day 14: 7.72 ± 0.40 Day 21: 8.69 ± 0.44 Day 28: 9.69 ± 0.48	Day 0: 2.4 ± 0.04 Day 1: 2.56 ± 0.05 Day 7: 2.7 ± 0.04	SF/H Day 0: 2.49 ± 0.05 Day 1: 2.6 ± 0.06 Day 7: 2.78 ± 0.04
Shao Y. F. et al., 2024 [34]	91 ± 4%	b-HA/SF 81 ± 2%	25−75 μm	b-HA/SF 25−75 μm	N.A.	N.A.	N.A.	N.A.	N.A.	N.A.	0.5 h: 566.17 ± 35.32 1 h:	b-HA/SF 0.5 h: 278.28 ± 117.72 1 h: 304.97	N.A.	N.A.

(*continued on next page*)

Table 3 (*continued*)

First Author and Year	Porosity		Pore size		Compressive modulus		Compressive Strength		Water Uptake (%)		Swelling Ratio (%)		Scaffold Degradation (%)	
	Control Group	Intervention Groups	Control Group	Intervention Groups	Control Group	Intervention Groups	Control Group	Intervention Groups	Control Group	Intervention Groups	Control Group	Intervention Groups	Control Group	Intervention Groups
											577.59 ± 37.79 2 h: 580.76 ± 55.144 h: 590.11 ± 53.90 8 h: 612.28 ± 42.13 12 h: 613.38 ± 50.80 24 h: 644.23 ± 42.12 72 h: 724.23 ± 37.16 168 h: 840.15 ± 45.84	± 65.67 2 h: 318.07 ± 57.62 4 h: 331.12 ± 48.95 8 h: 357.86 ± 51.43 12 h: 361.01 ± 46.47 24 h: 379.05 ± 47.71 72 h: 434.26 ± 33.45 168 h: 468.42 ± 17.34		
Tang Z. et al., 2024 [38]	46.92%	HA 46.92%	28.3 ± 6.09 μm	HA 28.3 ± 6.09 μm	N.A.	N.A.	N.A.	N.A.	N.A.	N.A.	N.A.	N.A.	N.A.	N.A.
Yan L. P. et al., 2014 [32]	N.A.	N.A.	Macropores: 300–700 μm; Micropores: <50 μm	SC16 Macropores: 300–700 μm; Micropores: <50 μm	Before cell culturing: 0.41 ± 0.10 MPa; after cell culturing 0.69 ± 0.10 MPa	SC16 Before cell cultiring: 0.40 ± 0.08 MPa; after cell culturing: 0.72 ± 0.13 MPa	N.A.	N.A.	N.A.	N.A.	N.A.	N.A.	12h:15 Day 1: 20 Day 2: 25 Day 7: 40	SC16 12h: 8 Day 1: 13 Day 2: 15 Day 7: 20
Yu X. et al., 2021 [41]	92.63	nHA/SF 87.80	N.A.	N.A.	0.14 ± 0.026 MPa	nHA/SF 0.22 ± 0.01 MPa	N.A.	N.A.	N.A.	N.A.	N.A.	N.A.	With protease: Day 1: 84 Day 3: 68.8 Day 5: 58.8 Day 7: 54.8 Day 10: 42.3; Without protease: Day 1: 92.3 Day 3: 73.9 Day 5: 67.5 Day	nHA/SF With protease: Day 1: 74 Day 3: 47.16 Day 5: 41.13 Day 7: 28.8 Day 10: 17.8; Without protease: Day 1: 91.9 Day 3: 74.5 Day 5: 64.3 Day 7: 53.7 Day 10: 44.1

(*continued on next page*)

Table 3 (*continued*)

First Author and Year	Porosity		Pore size		Compressive modulus		Compressive Strength		Water Uptake (%)		Swelling Ratio (%)		Scaffold Degradation (%)	
	Control Group	Intervention Groups	Control Group	Intervention Groups	Control Group	Intervention Groups	Control Group	Intervention Groups	Control Group	Intervention Groups	Control Group	Intervention Groups	Control Group	Intervention Groups
													7: 58.8 Day 10: 53.6	
Zhu Y. et al., 2024 [40]	N.A.	N.A.	Seedbeed 181.17 ± 83.74 nm. SF 97.53 ± 28 0.13 nm. OxSF 65.15 ± 19.70 nm	OxSF/ACP 87.24 ± 43.19 nm	N.A.	N.A.	SF: 5.1 ± 0.89 kPa; Ox SF: 1.80 ± 1.24 kPa	Ox SF ACP: 5.35 ± 2.44 kPa Ox SF ACP PRP: 13.94 ± 2.77 kPa	N.A.	N.A.	N.A.	N.A.	4 days: SF: 65.80; Ox SF: 64.66; 7 days: SF: 61.94; Ox SF:57.58; 14 days: SF: 56.07; Ox SF: 55.84	4 days: Ox SF ACP: 73.16 Ox SF ACP PRP: 36.15; 7 days: Ox SF ACP: 67.23 Ox SF ACP PRP: 25.85; 14 days: Ox SF ACP: 64.58; Ox SF ACP PRP: 23.66

drying for 72 h, both at 37 °C [35].

Salt leaching was utilized in four studies to produce SF based materials with a porous morphology [30,32,33,39]. In two cases, SF electrospinning was exploited to obtain scaffolds. Ko et al. dispersed GPTMS-HAp into the SF solution and added Poly(ethylene oxide) (PEO) prior to the electrospinning step to enhance the compound stability. The resulting fibers were then lyophilized leading to 3D SF scaffolds available for further functionalization steps [46]. Tang et al. produced a double faced material consisting of an inner layer composed by SF/PCL/HAp and an outer layer composed by SF/PCL/Se. Both layers were fabricated by dissolving respective components in 1,1,1,3,3,3 HFIP, which was electrospun and finally crosslinked in anhydrous ethanol. The two layers were then assembled by hot pressing at 20 MPa and 80 C in order to produce a faced material consisting of an inner layer composed by SF/PCL/HAp and an outer layer composed by SF/PCL/Se [38].

Shao et al. utilized a distinct synthesis approach based on electric field-induced gelation. In this method, aqueous HAp/SF dispersions were subjected to electrodeposition under a constant potential within an electrolytic cell. Composite hydrogels with varying HA contents were formed using graphite as both the working and counter electrodes, applying a voltage of 25 V for 25 min at room temperature. The resulting HAp/SF gels were then frozen overnight at −20 °C and subsequently lyophilized for 48 h [34].

In the work from Zhu et al., a sonication step performed at 50 % amplitude for 15 s was the initiating agent for producing a composite hydrogel, allowing the formation of a SF and OxSF network [40].

Lyu et al. synthetized composite SF-HAp coatings through the deposition of supersaturated ions (Zn^{2+}/Ca^{2+} and Mg^{2+}/Ca^{2+}) into a SF-based solution. Specifically, the pH-adjusted electrolyte solution was prepared, and electrochemical deposition was carried out using a three-electrode system comprising a platinum anode, a saturated calomel reference electrode, and an SF-coated titanium cathode. Transient electrochemical methods were employed at room temperature. Following ion deposition, the mineralized SF composite membranes were thoroughly rinsed and air-dried [47].

Only in the paper of Park et al. we have found a scaffold's different production method. In particular, in this study silk sutures were commercially purchased and scaffolds produced using a weaving machine. The weaved raw silk materials were afterward elaborated through a degumming step to extract sericin and then soaked in a collagen solution prior to a final lyophilization phase [37].

3.4. Morphological and mechanical characteristics

Porosity and pore size of the SF based materials represent pivotal factors to be kept into consideration, considering that these parameters crucially affect the cell's tendency to populate and proliferate within the scaffolds. Not all the selected studies clearly reported quantitative assesment of these parameters, although providing images showing the internal morphology.

Available porosity and average pore size values are reported in Table 3. Globally, these two parameters are strongly affected by production methodology, SF concentration, number and nature of additional components and dispersion level of the calcium-based material. It is worth noting that the porosity percentages, when compared with the production method, show degree of variability (ranging on average from 40 to 88%). It is therefore impossible to establish a clear correlation between such parameters, due to the limited number of available cases. When considering the addition of calcium-based composites as a parameter influencing the scaffold porosity, we observed a slight increase in porosity resulting from the incorporation of calcium derivatives. The only exceptions were observed in the work from Pina et al. [30] where the addition of β-TCP lowered material porosity from 64.70 ± 2.05 of SF control scaffold to 39.60 ± 8.70 of the SF/β-TCP compound, and in the paper of Yu et al., whereas the integration of

NG/GMs/nHAp/to SF decreased porosity on average from 92% to 67% [41]. Pores' size is also affected by great variability, with pores dimensions ranging from 20 to 700 μm Table 3. The fabrication technique was the main component affecting the pores size, and above all in studies utilizing the salt leaching approach, pores ranging from 270 to 700 μm were detected, with a larger mean size compared to that of artifacts by other production techniques [30–32,39]. On the contrary, 3D structures prepared via only a conventional freeze-drying approach were characterized by a smaller pore size, ranging from 25 to about 100 μm [34,43,45].

Mechanical performances of the SF composite scaffolds were examined. We have found discrepancies among the considered studies, deriving from the diverse manufacturing/measuring techniques and employed setups. The results highlighted different mechanical values and behaviors, in some cases high compressive modulus values have been found, as for example in the paper from Pina et al. where the sample SF/MnTCP showed a compressive modulus of 21 MPa [30]. On the other hand, Huang et al. measured a compressive modulus with highly lower values, *i.e.* 1,5 MPa in SF/nHAp sample [33]. The same concerns to measurements reporting the compressive strength, ranging in calcium composites-loaded samples from 2.1 kPa to 5.4 MPa [30,36]. These frequently observed dissimilarities can be hypothetically attributable not only to different experimental measurements setups, but also to variations in shape of the manufactured scaffolds, as well as to their composition and internal morphology. 2 out 19 studies also performed mechanical measurements of samples in wet conditions; in particular, the second study conducted measurements prior to and following cell culture [30,33].

Two studies analyzed the scaffolds' hydrophilicity, a parameter indicative of their interaction with biological fluids and essential for facilitating cellular migration into them. The resulting percentage values water uptake are reported in Table 3 and in both instances water uptake decreases with the addition of calcium-based compounds. Specifically, Park et al. reported a decrease of water uptake from 95.88 % in SF control scaffolds to 77.94 % for SF-β-TCP scaffolds loaded with medium-sized granules of β-TCP [43]. In Kim et al.'s work, an even greater decrease in the percentage of adsorbed water was detected, going from about 90% in SF controls to about 75% in SF/nHAp samples, which is due to the lower water absorption capability of HAp fillers [31]. Some studies also analyzed the swelling ratio, a parameter intimately related to water uptake. Combined swelling values in percentage after 24h of water exposure, are shown in Table 3. A swelling decrease tendency deriving from the addition of calcium-based materials, was validated as a general trend for the analyzed systems.

The last factor we considered as indicative of scaffolds' reliability was their degradation tendency, critical for materials application in cell culture and implantation. 5 out of 19 studies analyzed scaffolds degradation with or without the presence of protease. Specifically, in three studies the degradation rate was estimated by treating the materials in PBS or distilled water in presence of proteases of different nature, at different times of exposure [32,40,41]. In the remaining studies, degradation rate was estimated only exposing the SF based-scaffolds to PBS without proteases and measuring their auto-degradation rate. Degradation is assessed by estimating material's percentage weight loss ratio after treatment of scaffolds, however the timing of exposures in the different analyzed cases are variable and extended over a large time scale, being included between 3 h and 8 weeks [30,41,44]. It is evident how, in different cases, the addition of calcium-based materials resulted in reduced weight loss ratio in the samples, mainly because of the altered material morphology, enhanced presence of crystalline structures/components and molecular affinity between calcium composites and SF molecules [30,32].

3.5. Biological testing

To critically assess the biological performance and translational potential of SF scaffolds enriched with calcium-based fillers, a wide range of *in vitro* and *in vivo* evaluation strategies has been reported in the literature. These experimental approaches are essential to elucidate not only the cytocompatibility of the developed materials, but also their ability to promote cell proliferation, osteogenic differentiation, and ultimately functional tissue regeneration. In this context, Fig. 3 provides a comprehensive and introductive overview of the main biological models and analytical methods adopted in the studies included in this systematic review, highlighting the multiscale experimental framework through which SF scaffolds enriched with CaP based materials are currently investigated, from preliminary biological screening to preclinical evaluation.

3.5.1. *In vitro* biological testing

The *in vitro* studies included in this systematic review highlighted the central role of calcium-based materials in terms of proliferation and differentiation, once combined with a SF matrix, as detailed in Fig. 3. Most of the analyzed studies employed bone-marrow mesenchymal stem cell (BMSCs) [23,31,33,39–42,44]and human mesenchymal stem cell (hMSCs) [36,43]as elected model to better understand the cellular reaction to composite materials. Fewer studies tested the versatility of these scaffolds on animal cellular models, such as MC3T3-E1 pre--osteoblasts alone [34,35,45] and co-cultured with gingival fibroblasts [38].

Noteworthy, human adipose-derived stem cells (hASC) have been employed in two of the selected studies, highlighting that the synthetic structures were not only suitable substrates for bone-like cells, but also for other lineages that can lead to bone formation [30,32].

3.5.1.1. Proliferation trends across studies. The impact of the synthetic bone substitutes on cellular proliferation has been evaluated through different tests; MTS, CCK-8, and MTT were the most employed assays to measure metabolic activity as an index of cell proliferation, as better detailed in Table 4. All the tests have been performed at different points in time, ranging from 1 to 28 days. Only Kim et al. analyzed the proliferative outcome at one single time point, *i.e.* six days after cell seeding [36].

In detail, MTS assays performed by Liu et al. and Kim et al. underlined a positive trend up to 7 days in control and intervention groups, thus highlighting that a neat SF matrix is a suitable substrate for BMSCs proliferation [39]. Nevertheless, a follow-up study by Kim et al. showed how this aspect that can be further improved by incorporating nHAp particles, with concentration in weight ranging between 0% and 3%,in a SF hydrogel structure, which consistently increased the optical density (OD) over time compared to the control group [36]. Within this experimental scenario, OD values also revealed that hMSCs proliferation, if compared to the control group, was strongly supported by the presence of the ceramic material; nevertheless, no significant differences were found between 2% and 3% wt concentration.

Interestingly, Park et al. analyzed the impact of particle size in affecting cellular proliferation combining β-TCP particles ranging from 300 to 600 nm (small granule size - GS) and 600–900 nm (medium granule size - GM) in a SF-matrix, with 1:1 of mixing ratio. All the results reported by the analyzed studies demonstrated an increased metabolic activity of hMSCs up to the seventh day of colture, with a similar growing pattern among the samples. This importantly reveals that size features of β-TCP nanoparticles does not affect cellular proliferation, while maintaining a non-cytotoxic behavior [43].

BMSCs have been widely used as cellular model to analyze the effectiveness of different SF/β-TCP concentrations. Jing et al., tested three different SF/β-TCP ratios (1:2, 1:1, 2:1). Among the groups, the same concentration of SF/β-TCP named as SF/β-TCP (1:1) seemed to boost BMSCs proliferation after only 24 h, reaching the highest OD value (1.54 ± 0.13 OD at 450 nm on Day 7) compared to the SF (1.12 ± 0.11), SF/β-TCP (2:1) (1.41 ± 0.10) and SF/β-TCP (1:2) (1.40 ± 0.11) groups.

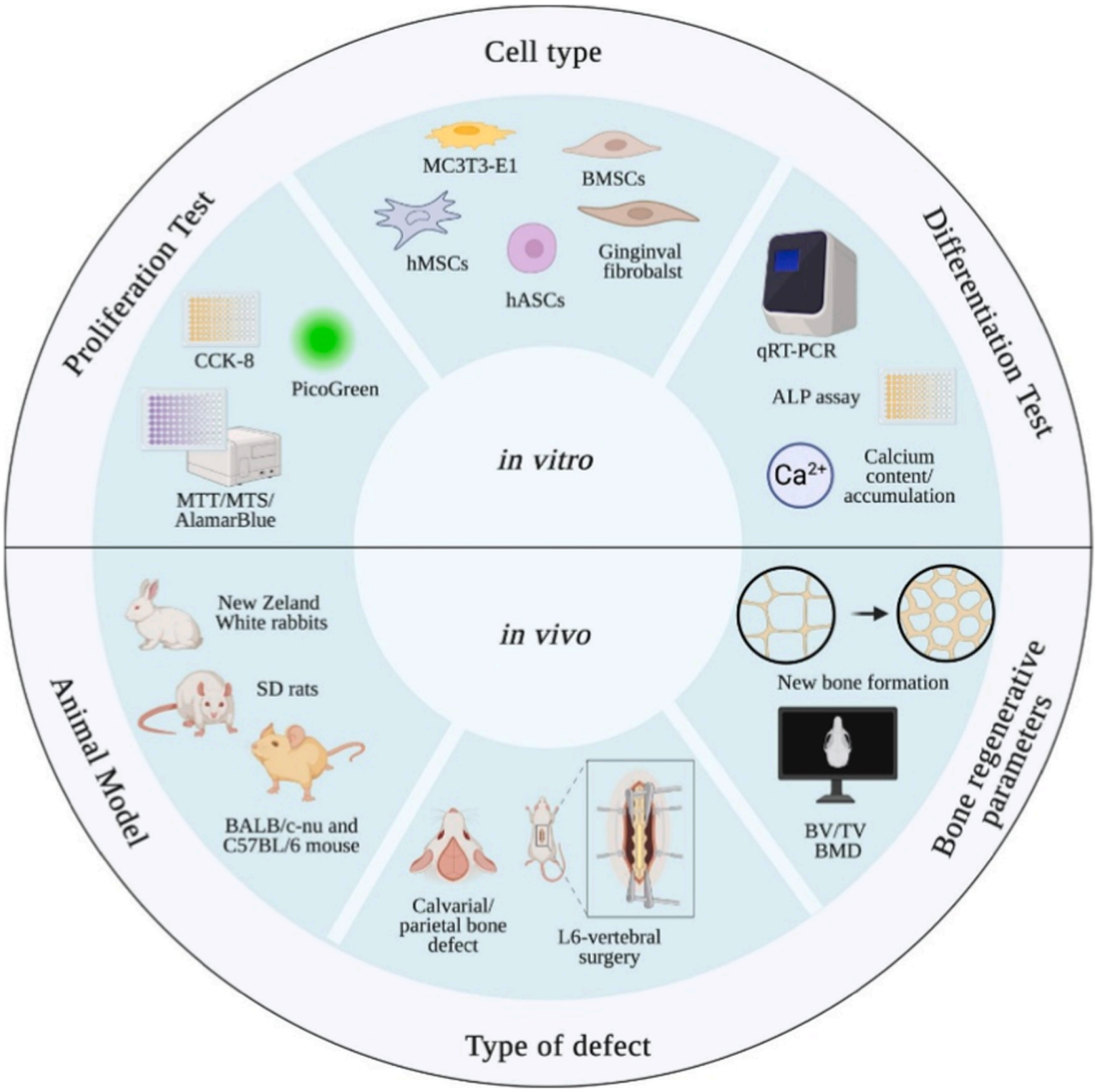

Fig. 3. Schematic description of the main characteristics of *in vitro* and *in vivo* studies included in the systematic review. Murine pre-osteoblasts (MC3T3-E1); Human mesenchymal stem cells (hMSCs); Human adipose-derived stem cells (hASCs); Bone marrow stem cells (BMSCs); Sprangue Dawley rats (SD rats); Percentage bone volume (BV/TV); Bone mineral density (BMD). Created in https://BioRender.com.

This result suggests that a particular attention to the balance between organic and inorganic components in scaffold composition, plays a crucial role in optimizing cell proliferation [31,44].

The positive proliferation trend for BMSCs has been also confirmed by other studies, which analyzed the role of different calcium-based materials coupled with additive factors. Kim et al., demonstrated that a concentration of 10% HAp could further improve cellular growth on all the surfaces, with a higher value on SF/TiO_2/HA structures compared to SF scaffolds, indicating that TiO_2 not only enhanced scaffolds' mechanical features, but also their biological properties [31].

The role of additional component in BMSCs behavioral modulation has been also confirmed by Liu et al. and Yu et al. Both studies demonstrated that SPI and GO together and combined with β-TCP or with gelatin microspheres and nHAp, actually supported cell adhesion at 24h, leading to the highest cell viability on the composite scaffolds at the end of the experimental time points (7 and 10 days, respectively). Liu et al., justified the slight BMSCs proliferation with the hypothesis that SF scaffolds surfaces did not presented enough surface receptors assisting cell adhesion and spreading [23,41].

Interestingly, Tang et al., co-coltured pre-osteoblasts (MC3T3-E1) and gingival fibroblasts onto a double layered scaffold able to mimic the natural morphology of periosteum: both layers of the scaffold at 24h demonstrated a firmly cellular adhesion of the selected cells. Moreover, MC3T3-E1 on HAp-loaded material displayed a cellular activity comparable to the one of controls, from 1 to 5 days after cell seeding, hence reaching a peak of proliferation at day 5 on the samples loaded with HAp and the lower concentration of SeNPs, here employed as antimicrobial agent, although with a mechanism of action not yet entirely clear. In this case, the authors attributed this behavior not to the presence of the ceramic powder itself but rather to the SeNPs, as selenium is a micronutrient with a proven involvement in proliferation in a huge variety of cells as macrophages, fibroblasts and endothelial cells. In this light, the same considerations can be proposed for gingival fibroblasts. On the contrary, in higher amounts, SeNPs could negatively affect cell metabolism [38]. Shahid et al., confirmed the results obtained by Tang's groups. In particular, a trend of decreasing viability from day 1 to day 3 was observed in MC3T3-E1 cells, followed by an increase at day 5. As stated by the authors, the initial decrease of metabolic activity reflects

Table 4
In vitro results obtained across studies included in the systematic review. Data includes resulta related to cellular proliferation and differentiation toward the osteoblastic lineage for the control and intervention groups. Abbreviations employed: Silk Fibroin (SF); Octacalcium Phosphate (OCP); β -Tricalcium Phosphate (β-TCP); Hydroxyapatite (HA or Hap or HAP); Nano-hydroxyapatite (nHAp); Poly(vinylpyrrolidone) (PVP); Poly-dopamine (PDA); Soy Protein Isolate (SPI); Graphene Oxide (GO); Primary Dental Pulp Cells (DPCs); Calcium Phosphate (CaP); Amorphous Calcium Phosphate (ACP); Not applicable (N.A.).

First Author and Year	Cell Type	Cellular proliferation						Cellular differentiation						Main outcomes
		Test and experimental time point	Control Group	Intervention Group 1	Intervention Group 2	Intervention Group 3	Intervention Group 4	Test and experimental time point	Control Group	Intervention Group 1	Intervention Group 2	Intervention Group 3	Intervention Group 4	
Han F. et al., 2019 [45]	MC3T3-E1	CCK-8 assay (OD 450 nm); 2-4-6 days	Day 2: 0.19 ± 0.05; Day 4: 0.30 ± 0.02; Day 6: 0.59 ± 0.02;	SF/OCP Day 2: 0.19 ± 0.04; Day 4: 0.29 ± 0.06; Day 6: 0.60 ± 0.05;	N.A.	N.A.	N.A.	N.A.; N.A.	N.A.	N.A.	N.A.	N.A.	N.A.	MC3T3-E1 cells could rapidly adhere and proliferate on SF and SF/OCP scaffolds surface with no statistical differences between the two group at the same time points.
Huang X. et al., 2014 [33]	BMSCs	PicoGreenTM DNA Assay (ng/ml); 1-3-6-9-12 days	Day 1: 99.06 ± 8.82; Day 3: 144.34 ± 46.08; Day 6:288.66 ± 59.80; Day 9:393.10 ± 10.78; Day 12:429.25 ± 46.09;	SF-A20HA: Day 1:114.45 ± 20.59; Day 3:124.10 ± 50.98; Day 6:227.57 ± 25.49; Day 9:296.08 ± 18.63; Day 12:421.44± 10.78;	SF-D20HA: Day 1:107.29 ± 6.86; Day 3:165.31 ± 47.06; Day 6:328.91 ± 23.53; Day 9:482.05 ± 23.53; Day 12:514.93 ± 27.45;	SF-A40HA: Day 1:114.84 ± 8.82; Day 3:157.17 ± 9.81; Day 6:325.02 ± 4.90; Day 9:520.98 ± 7.85; 12day:590.13 ± 4.90;	SF-D40HA: Day 1:97.87 ± 6.86; Day 3:184.98 ± 8.82; Day 6:432.24 ± 4.90; Day 9:594.86 ± 9.80; Day 12:659.12 ± 7.84;	ALP activity (mmol pNPP/ hour/mg protein); 1-7-14-28 days	Day 1: 0.62 ± 0.03; Day 7: 0.92 ± 0.08; Day 14: 1.26 ± 0.12; Day 28: 1.69 ± 0.11;	SF-A20HA: Day 1: 0.63 ± 0.21; Day 7: 2.65 ± 0.14; Day 14: 1.53 ± 0.16; Day 28: 1 ± 0.10;	SF-D20HA Day 1: 0.62 ± 0.05; Day 7: 3.2 ± 0.10; Day 14: 2.13 ± 0.34; Day 28: 1.18 ± 0.48;	SF-A40HA Day 1: 1.02 ± 0.06; Day 7: 4.01 ± 0.18; Day 14: 2.41 ± 0.59; Day 28: 1.52 ± 0.3;	SF-D40HA: Day 1: 1.35 ± 0.09; Day 7: 5.36 ± 0.59; Day 14: 3.89 ± 0.25; Day 28: 1.67 ± 0.42;	Silk/HA nanoparticles scaffolds showed improved osteogenic activity and cell compatibility compared to silk/HA scaffolds, reaching up to 40% HA without compromising the mechanical properties of biomaterial.
								Calcium content (μg/ scaffold); 1-7-14-28 days	Day 1: 1 ± 0.14; Day 7: 1.44 ± 0.22; Day 14: 1.45 ± 0.33; Day 28: 3.01 ± 0.18;	SF-A20HA Day 1: 0.97 ± 0.42; Day 7: 2.03 ± 0.33; Day 14: 6.88 ± 2.51; Day 28: 15.00 ± 4.13;	SF-D20HA Day 1: 0.87 ± 0.23; Day 7: 2.48 ± 0.84; Day 14: 10.04 ± 0.33; Day 28: 18.08 ± 0.47;	SF-A40HA Day 1: 1.94 ± 0.28; Day 7: 5.63 ± 0.51; Day 14: 13.32 ± 0.98; Day 28: 23.87 ± 1.44;	SF-D40HA: Day 1: 2.20 ± 0.79; Day 7: 7.42 ± 0.93; Day 14: 15.34 ± 2.18; Day 28: 27.51 ± 1.07;	
								OC Gene Expression (fold change); 1-7-14-28 days	day 1: 0.94 ± 0.13; day 7: 0.98 ± 0.18; day 14: 1.2 ± 0.12; day 28: 1.80 ± 0.10;	SF-A20HA: day 1: 1.72 ± 0.12; day 7: 2.85 ± 0.53; day 14: 3.96 ± 0.89; day 28: 8.10 ± 1.26;	SF-D20HA day 1: 1.02 ± 0.15; day 7: 1.88 ± 0.27; day 14: 4.45 ± 0.59; day 28: 9.56 ± 2.24;	SF-A40HA: day 1: 1.24 ± 0.10; day 7: 3.18 ± 0.55; day 14: 6.85 ± 0.88; day 28: 12.02 ± 2.49;	SF-D40HA day 1: 1.96 ± 0.21; day 7: 3.72 ± 0.71; day 14: 9.03 ± 0.98; day 28: 16.20 ± 2.88;	
								RUNX2 Gene Expression (fold change); 1-7-14-28 days	day 1: 0.77 ± 0.01; day 7: 1.04 ± 0.09; day 14:	SF-A20HA: day 1: 1.11 ± 0.48; day 7: 3.64 ± 0.55; day 14:	SH-D20HA day 1: 1.02 ± 0.11; day 7: 4.60 ± 0.260; day	SF-A40HA day 1: 1.75 ± 0.17; day 7: 5.13 ± 0.9; day 14:	SF-D40HA day 1: 2.28 ± 0.18; day 7: 7.62 ± 1.13; day 14:	

(*continued on next page*)

Table 4 (*continued*)

First Author and Year	Cell Type	Cellular proliferation						Cellular differentiation						Main outcomes
		Test and experimental time point	Control Group	Intervention Group 1	Intervention Group 2	Intervention Group 3	Intervention Group 4	Test and experimental time point	Control Group	Intervention Group 1	Intervention Group 2	Intervention Group 3	Intervention Group 4	
									1.53 ± 0.09; day 28: 1.74 ± 0.12;	2.42 ± 0.07; day 28: 0.92 ± 0.03;	14: 2.25 ± 0.55; day 28: 0.71 ± 0.04;	2.14 ± 0.69; day 28: 0.54 ± 0.04;	2.22 ± 0.75; day 28: 0.54 ± 0.03;	
Jing T. et al., 2022 [44]	BMSCs	CCK-8 assay (OD 450 nm); 1-3-5-7 days	Day 1: 0.42 ± 0.04; Day 3: 0.60 ± 0.06; Day 5: 1.06 ± 0.06; Day 7: 1.12 ± 0.11:	SF/β-TCP (2/1) Day 1: 0.52 ± 0.06; Day 3: 0.71 ± 0.09; Day 5: 1.18 ± 0.09; Day 7: 1.41 ± 0.10:	SF/β-TCP (1/1) Day 1: 1.21 ± 0.03; Day 3: 0.70 ± 0.06; Day 5: 1.45 ± 0.04; Day 7: 1.54 ± 0.13:	SF/β-TCP (1/2) Day 1: 0.20 ± 0.07; Day 3: 0.56 ± 0.06; Day 5: 1.17 ± 0.09; Day 7: 1.40 ± 0.11:	N.A.	ALP activity (absorbance at 405 nm); 3-7-14 days	Day 3: 0.27 ± 0.05; Day 7: 0.62 ± 0.08; Day 14: 0.99 ± 0.062;	Day 3: 0.63 ± 0.05; Day 7: 0.75 ± 0.04; Day 14: 0.95 ± 0.14;	Day 3: 0.34 ± 0.04; Day 7: 0.76 ± 0.06; Day 14: 0.93 ± 0.07;	Day 3: 0.75 ± 0.05; Day 7: 1.14 ± 0.04; Day 14: 1.15 ± 0.21;	N.A.	The incorporation of β-TCP nanoparticles positively influenced cell proliferation. Specifically, SF scaffolds had a lower viability compared to the other three groups. ALP activity increased in all groups until day 7 but slightly decrease at day 14 with no statistical differences among the SF-based groups. At day 7, SF/β-TCP (1/2) scaffolds showed the highest ALP activity among SF-based groups.
Kim J. H. et al., 2015 [31]	BMSCs	CCK-8 assay (Absorbance 450 nm); 1-3-7 days	Day 1:0.012 ± 0.01; Day 3:0.06 ± 0.00; Day 7: 0.14 ± 0.01	SF/HA: Day 1:0.038 ± 0.00; Day 3:0.08 ± 0.01; Day 7: 0.163 ± 0.009	SF/TiO_2/HA Day 1:0.032 ± 0.00; Day 3:0.1 ± 0.01; Day 7: 0.17 ± 0.02	N.A.	N.A.	ALP activity mmol pNPP/hour/mg protein; 1-7-14 days	day 1: 0.34 ± 0.04; day 7: 0.85 ± 0.01; day 14: 0.19 ± 0.02	SF/HA: day 1: 0.96 ± 0.08; day 7: 1.17 ± 0.06; day 14: 0.55 ± 0.04	SF/TiO_2/HA: day 1: 0.91 ± 0.02; day 7: 1.50 ± 0.02; day 14: 0.94 ± 0.01	N.A.	N.A.	SF/TiO_2/HA demonstrated improved mechanical properties compared to SF and SF/HA scaffolds as well as enhanced cell infiltration, proliferation and osteogenic activity
								OCN gene expression (fold change); 14 days	1.042 ± 0.00	0.97 ± 0.03	0.99 ± 0.00	N.A.	N.A.	
								COL-I gene expression (fold change); 14 days	6.47 ± 0.46	1.80 ± 0.1	2.74 ± 0.30	N.A.	N.A.	
								RUNX-2 gene expression (fold change); 14 days	19.47 ± 1.31	34.81 ± 0.01	5.31 ± 0.14	N.A.	N.A.	
Kim M. H. et al., 2017 [36]	hMSCs	MTS assay (OD 490 nm); 6 days	0.35 ± 0.09	SF-1 0.46 ± 0.07	SF-2 0.61 ± 0.08	SF-3 0.57 ± 0.09	N.A.	ALP activity (nmol/30 min/mg of protein); 7 days	1.50 ± 0.64	SF-1 1.91 ± 0.48	SF-2 3.07 ± 0.39	SF-3 3.05 ± 0.38	N.A.	The proliferation and osteogenic activity of hMSCs increased with higher HAP concentrations, with no significant difference observed
								Calcium accumulation	1.00 ± 0.00	1.61 ± 0.32	3.11 ± 0.51	3.31 ± 0.31	N.A.	

(*continued on next page*)

Table 4 (*continued*)

First Author and Year	Cell Type	Cellular proliferation						Cellular differentiation						Main outcomes
		Test and experimental time point	Control Group	Intervention Group 1	Intervention Group 2	Intervention Group 3	Intervention Group 4	Test and experimental time point	Control Group	Intervention Group 1	Intervention Group 2	Intervention Group 3	Intervention Group 4	
								(Fold change); 21 days						between SF-2 and SF-3.
Lee D. et al., 2017 [42]	BMSCs	MTT assay (Optical Intensity 570 nm); 1-7-14-21-28 days	SF: Day 1: 0.58 ± 0.01; Day 7:0.62 ± 0.03; Day 14:0.63 ± 0.02; Day 21:0.59 ± 0.02; Day 28:0.65 ± 0.01;	SF75/ β-TCP25: Day 1:0.55 ± 0.03; Day 7:0.55 ± 0.03; Day 14:0.61 ± 0.04; Day 21:0.60 ± 0.02; Day 28:0.60 ± 0.01;	SF50/ β-TCP50: Day 1:0.55 ± 0.04; Day 7:0.57 ± 0.03; Day 14:0.60 ± 0.02; Day 21:0.59 ± 0.04; Day 28:0.59 ± 0.02;	SF25/β-TCP75: Day 1: 0.55 ± 0.03; Day 7: 0.58 ± 0.05; Day 14: 0.60 ± 0.04; Day 21: 0.55 ± 0.02; Day 28: 0.58 ± 0.01;	N.A.	ALP activity (Optical Intensity 450 nm); 1-7-14-21-28 days	SF: Day 1: 0.57 ± 0.00; Day 7: 0.58 ± 0.01; Day 14: 0.62 ± 0.02; Day 21: 0.61 ± 0.03; Day 28: 0.68 ± 0.04;	SF75/ β-TCP25: Day 1: 0.56 ± 0.03; Day 7: 0.57 ± 0.02; Day 14: 0.58 ± 0.04; Day 21: 0.59 ± 0.02; Day 28: 0.59 ± 0.02;	SF50/ β-TCP50: Day 1: 0.55 ± 0.04; Day 7: 0.55 ± 0.02; Day 14: 0.58 ± 0.01; Day 21: 0.59 ± 0.03; Day 28: 0.59 ± 0.02;	SF25/ β-TCP75: Day 1: 0.54 ± 0.01; Day 7: 0.54 ± 0.01; Day 14: 0.56 ± 0.01; Day 21: 0.58 ± 0.05; Day 28: 0.59 ± 0.02	N.A.	SF/β-TCP scaffolds promoted higher BMSC proliferation and osteogenic differentiation compared to the control as demonstrated by ALP activity. This behavior is particularly clear on SF75/β-TCP25 scaffolds.
								RT-PCR (mRNA expression normalized by GAPDH); 28 days	SF: ColI:1.10 ± 0.01; OCN:1.380 ± 0.01; RUNX 2:1.38 ± 0.00	SF75/ β-TCP25: ColI:1.65 ± 0.02; OCN:1.62 ± 0.2; RUNX 2:1.69 ± 0.00;	SF50/ β-TCP50 ColI:1.15 ± 0.01; OCN:1.43 ± 0.02 RUNX 2:1.25 ± 0.00;	SF25/ β-TCP75 ColI:0.82 ± 0.01 OCN:0.92 ± 0.00 RUNX 2: 0.96 ± 0.00;	N.A.	
Liu F. et al., 2020 [23]	BMSCs	CCK-8 assay (Absorbance 450 nm); 1-3-5-7 days	Day 1 87.99 ± 2.57; Day 3:95.09 ± 2.74; Day 5:87.82 ± 2.31; Day 7: 81.57 ± 0.69	SF/SPI/β-TCP Day 1:86.99 ± 3.42; Day 3:99.91 ± 3.08; Day 5:90.45 ± 5.14; Day 7; 94.24 ± 2.91	SF/SPI/ β-TCP/GO Day 1:96.23 ± 5.22; Day 3:104.79 ± 2.31; Day 5:108.62 ± 5.65; Day 7: 112.67 ± 3.08	N.A.	N.A.	ALP activity (DEA); 1-3-5-7 days	Day 1: 0.26 ± 0.00; Day 3: 0.15 ± 0.01; Day 5: 0.58 ± 0.06; Day 7: 1.02 ± 0.02	SF/SPI/ β-TCP: Day 1: 0.61 ± 0.08; Day 3: 0.42 ± 0.06; Day 5: 1.00 ± 0.03; Day 7; 1.13 ± 0.01	SF/SPI/ β-TCP/GO Day 1: 0.24 ± 0.1; Day 3: 0.23 ± 0.02; Day 5: 1.99 ± 0.11; Day 7: 1.10 ± 0.04	N.A.	N.A.	The incorporation of β-TCP and GO improved mechanical and biological properties of SF-based scaffolds, specifically BMSCs adhesion, proliferation, osteogenic differentiation and bio-mineralization
								RUNX-2 expression (fold change); 7–14 days	Day 7: 2.29 ± 0.33; Day 14: 2.19 ± 0.42	SF/SPI/ β-TCP: Day 7: 3.17 ± 0.52; Day 14: 4.87 ± 0.48;	SF/SPI/ β-TCP: Day 7: 4.99 ± 1.15; Day 14: 8.12 ± 0.54;	N.A.	N.A.	
								OC expression (fold change); 7–14 days	Day 7: 2.48 ± 0.31; Day 14: 5.08 ± 1.04	SF/SPI/ β-TCP: Day 7: 4.06 ± 0.88; Day 14: 5.30 ± 1;	SF/SPI/ β-TCP: Day 7: 5.70 ± 0.62; Day 14: 8.80 ± 0.87;	N.A.	N.A.	
								COL1 expression (fold Change); 7–14 days	Day 7: 4.56 ± 0.52; Day	SF/SPI/ β-TCP: Day 7: 5.45 ± 1.50;	SF/SPI/ β-TCP: Day 7: 8.55 ± 0.98;	N.A.	N.A.	

(*continued on next page*)

Table 4 (*continued*)

First Author and Year	Cell Type	Cellular proliferation						Cellular differentiation						Main outcomes
		Test and experimental time point	Control Group	Intervention Group 1	Intervention Group 2	Intervention Group 3	Intervention Group 4	Test and experimental time point	Control Group	Intervention Group 1	Intervention Group 2	Intervention Group 3	Intervention Group 4	
									14: 4.03 ± 0.67	Day 14: 7.82 ± 1.08;	Day 14: 12.62 ± 1.31;			
Liu H. et al., 2015 [50]	Rat BMSCs;	MTS assay (OD 490 nm); 1-3-5-7 days	Day 1: 0.04 ± 0.00; Day 3: 0.13 ± 0.00; Day 5: 0.17 ± 0.01; Day 7: 0.28 ± 0.01;	SF/nHAp Day 1: 0.05 ± 0.01; Day 3: 0.15 ± 0.00; Day 5: 0.18 ± 0.00; Day 7: 0.36 ± 0.02;	N.A.	N.A.	N.A.	ALP activity (OD 520 nm); 7–14 days	Day 7: 0.16 ± 0.03; Day 14: 0.20 ± 0.01;	SF/nHAp Day 7: 0.20 ± 0.02; Day 14: 0.36 ± 0.01;	N.A.	N.A.	N.A.	SF and SF-nHAp scaffolds favored cell attachment and proliferation of BMSCs *in vitro*, eliciting negligible inflammatory cell infiltration and underlining excellent scaffold bio-compatibility. SF-nHAp scaffolds showed an improved osteogenic potential compared to SF scaffolds and higher upregulation of osteogenesis related signaling pathways.
Lyu R. et al., 2025 [47]	hBMSCs	CCK-8 (OD value at 450 nm); 1-3-5 days	Day 1: 0.37 ± 0.10 Day 3: 0.52 ± 0.03 Day 5: 0.81 ± 0.12	SF/H Day 1: 0.44 ± 0.01 Day 3: 0.81 ± 0.12 Day 5: 1.54 ± 0.13	N.A.	N.A.	N.A.	ALP activity; 7–14 days	Day 7: 1.01 ± 0.00 Day 14: 2.07 ± 0.06	SF/H Day 7: 1.08 ± 0.67 Day 14: 3.04 ± 0.20	N.A.	N.A.	N.A.	hBMSCs proliferation rate seemed not be affected from the incorporation of HAp at day 1. At day 5 SF/H membranes presented a growth activity significantly higher than other groups. ALP results demonstrated not significant differences among SF and SF/H groups while RT-PCR revealed an up-regulation of OCN and COL-1 genes. No differences were detected for OPN.
								COL-1 expression (fold change); 21 days	2.43 ± 0.30	SF/H 6.02 ± 0.77	N.A.	N.A.	N.A.	
								RUNX-2 expression (fold change); 21 days	0.10 ± 0.00	SF/H 3.33 ± 0.40	N.A.	N.A.	N.A.	
								OPN expression (fold change); 21 days	8.01 ± 1.61	SF/H 10.97 ± 0.66	N.A.	N.A.	N.A.	
Park H. J. et al., 2016 [43]	hMSC	CCK-8 assay (OD 450 nm); 1-7-14 days	Day 1:0.77 ± 0.04; Day 7:1.82 ± 0.08; Day 14:2.03 ± 0.02	GS Day 1:0.70 ± 0.02; Day 7:1.81 ± 0.01; Day 14:2.01 ± 0.04	GM Day 1:0.73 ± 0.04; Day 7:1.87 ± 0.03; Day 14:1.95 ± 0.05	N.A.	N.A.	N.A.; N.A.	N.A.	N.A.	N.A.	N.A.	N.A.	hMSCs metabolic activity increased from 1 to 7 days with no significant difference among the samples. Despite no toxic scaffold behavior, the addition of β-TCP microparticles into SF-nanofibers did not

(*continued on next page*)

Table 4 (*continued*)

First Author and Year	Cell Type	Cellular proliferation						Cellular differentiation						Main outcomes
		Test and experimental time point	Control Group	Intervention Group 1	Intervention Group 2	Intervention Group 3	Intervention Group 4	Test and experimental time point	Control Group	Intervention Group 1	Intervention Group 2	Intervention Group 3	Intervention Group 4	
														influence fibroblasts growth *in vitro*.
Pina S. et al., 2017 [30]	hASCs	Alamar Blue Assay (r.f.u.); 3-7-14 days	SF Day 3:60.56 ± 21.67; Day 7:147.87 ± 34.58; Day 14:87.92 ± 13.38	SF/β-TCP: Day 3:148.18 ± 17.52; Day 7:264.69 ± 44.26; Day 14:447.30 ± 111.59;	N.A.	N.A.	N.A.	ALP activity (μg/DNA); 14 days	SF in basal medium: 0.42 ± 0.06; SF in osteogenic medium: 0.95 ± 0.10	SF/β-TCP in basal medium: 0.65 ± 0.04 SF/β-TCP in osteogenic medium: 1.23 ± 0.10	N.A.	N.A.	N.A.	hASCs modulated their behavior in response to different doping agents; Zn presence led to an enhanced proliferation. Mg and Sr improved osteogenic activity and the combination of Sr and Zn led to an average influence on both cell proliferation and osteogenesis activity respect to single ions.
		Quant-iT PicoGreen dsDNA assay (μg/ml); 3-7-14-28 days	SF: Day 3: 0.01 ± 0.01; Day 7: 0.01 ± 0.00 Day 14: 0.012 ± 0.00; Day 28: 0.01 ± 0.00	SF/β-TCP: Day 3: 0.010 ± 0.00; Day 7: 0.01 ± 0.00; Day 14: 0.010 ± 0.00; Day 28: 0.06 ± 0.00	N.A.	N.A.	N.A.							
Shahid A. et al., 2024 [35]	MC3T3-E1	Alamar Blue Assay (% of TCP control); 1-3-5 days	Day 1: 96.90 ± 5.04 Day 3: 93.20 ± 4.80 Day 5: 110.80 ± 5.47	SF/H Day 1: 115.80 ± 5.71 Day 3: 93.50 ± 4.75 Day 5: 99.80 ± 4.99	N.A.	N.A.	N.A.	N.A.	N.A.	N.A.	N.A.	N.A.	N.A.	A trend of reduced viability has been observed from day 1 to day 3 for all scaffolds followed by an increase at day 5. HAp loaded scaffolds displayed a good cell viability on all the considered time points. No differences with the SF group were detected.
Shao Y. F. et al., 2024 [34]	MC3T3-E1	MTT (absorbance at 570 nm) 1-3-7 days	Day 1: 0.15 ± 0.02 Day 3: 0.15 ± 0.01 Day 7: 0.22 ± 0.02	b-HA/SF Day 1: 0.20 ± 0.03 Day 3: 0.21 ± 0.07 Day 5: 0.31 ± 0.04	N.A.	N.A.	N.A.	N.A.; N.A.	N.A.	N.A.	N.A.	N.A.	N.A.	b-HA/SF scaffolds are more favorable substrates for cell growth than SF scaffolds. After 7 days of static culture, b-HA/SF scaffolds showed a better cytocompatibility than b-SF
Tang Z. et al., 2024 [38]	MC3T3-E1	CCK-8 assay (OD value at 450 nm); 1-3-5 days	Day 1: 0.034 ± 0.002; Day 3:0.07 ± 0.01; Day 5: 0.075 ± 0.01	HA Day 1:0.033 ± 0.01; Day 3:0.073 ± 0.00; Day 5: 0.086 ± 0.00	N.A.	N.A.	N.A.	ALP activity (relative ALP expression); 7 days	1.10 ± 0.02	HA 1.23 ± 0.01	N.A.	N.A.	N.A.	The incorporation of nHA did not statistically improved proliferation rate of osteoblasts and gingival fibroblastic cells. On the other hand, nanofiber scaffolds containing
								OCN expression (relative mRNA	0.90 ± 0.07	HA 1.37 ± 0.21	N.A.	N.A.	N.A.	

(*continued on next page*)

Table 4 (*continued*)

First Author and Year	Cell Type	Cellular proliferation						Cellular differentiation						Main outcomes
		Test and experimental time point	Control Group	Intervention Group 1	Intervention Group 2	Intervention Group 3	Intervention Group 4	Test and experimental time point	Control Group	Intervention Group 1	Intervention Group 2	Intervention Group 3	Intervention Group 4	
								expression); 14 days						nHA exhibited singificantly elevated ALP levels.
	Gingival fibroblasts		Day 1:0.15 ± 0.01; Day 3:0.32 ± 0.04; Day 5: 0.80 ± 0.02	HA Day 1:0.15 ± 0.01; Day 3: 0.32 ± 0.01; Day 5: 0.82 ± 0.02				BSP expression (relative mRNA expression); 14 days	0.99 ± 0.06	HA 2.48 ± 0.09	N.A.	N.A.	N.A.	
								RUNX2 expression (relative mRNA expression); 14 days	0.89 ± 0.08	HA 1.36 ± 0.22	N.A.	N.A.	N.A.	
Yan L. P. et al., 2014 [32]	hASCS	Quant-iT PicoGreen dsDNA assay (μg/scaffold); 1-3-7-14 days	Day 1:0.99 ± 0.06; Day 3:1.45 ± 0.05; Day 7:1.68 ± 0.02; Day 14: 1.73 ± 0.05	SC16 Day 1:1.03 ± 0.02; Day 3: 1.46 ± 0.04; Day 7:1.66 ± 0.05; Day 14: 1.76 ± 0.06	N.A.	N.A.	N.A.	N.A.; N.A.	N.A.	N.A.	N.A.	N.A.	N.A.	S16 and SC16 scaffolds showed non-cytotoxic behavior as well as improved hASCs attachment, favored by microporous structure, viability and proliferation due to the presence of macropores. The culture of hASCS improved biomechanical features of both samples.
Yu X. et al., 2021 [41]	BMSC	CCK-8 assay (OD value at 450 nm); 1-3-7-10 days	Day 1; 0.79 ± 0.02: Day 3: 1.03 ± 0.10; Day 7: 1.24 ± 0.03 ; Day 10: 0.84 ± 0.01	nHA/SF Day 1: 0.81 ± 0.01: Day 3: 1.030 ± 0.06; Day 7: 1.28 ± 0.08; Day 10: 0.92 ± 0.06	N.A.	N.A.	N.A.	BMP-2 expression (relative mRNA expression); 3-7-10-14 days	Day 3: 0.99 ± 0.13; Day 7: 1.13 ± 0.07; Day 10: 1.26 ± 0.19; Day 14: 1.01 ± 0.03	nHA/SF Day 3: 1.19 ± 0.09; Day 7: 1.47 ± 0.10; Day 10: 4.58 ± 0.05; Day 14: 4.58 ± 0.03	N.A.	N.A.	N.A.	All the scaffolds significantly promoted BMSCs adhesion after 24h, but no significative differences can detected between SF and nHA/SF scaffolds. Higher levels of osteogenic proteins can be detected on nHA/SF group compared to SF group.
								OCN expression (relative mRNA expression); 3-7-10-14 days	Day 3: 1.22 ± 0.10; Day 7: 1.27 ± 0.10; Day 10: 0.68 ± 0.10; Day 14: 0.54 ± 0.12	nHA/SF Day 3: 1.32 ± 0.04; Day 7: 1.42 ± 0.04; Day 10: 0.79 ± 0.08; Day 14: 0.55 ± 0.06	N.A.	N.A.	N.A.	
								RUNX-2 expression	Day 3: 1.00 ±	nHA/SF Day 3:	N.A.	N.A.	N.A.	

(*continued on next page*)

Table 4 (*continued*)

First Author and Year	Cell Type	Cellular proliferation						Cellular differentiation						Main outcomes
		Test and experimental time point	Control Group	Intervention Group 1	Intervention Group 2	Intervention Group 3	Intervention Group 4	Test and experimental time point	Control Group	Intervention Group 1	Intervention Group 2	Intervention Group 3	Intervention Group 4	
								(relative mRNA expression); 3-7-10-14 days	0.07; Day 7: 1.26 ± 0.17; Day 10: 1.21 ± 0.04; Day 14: 0.98 ± 0.05	1.26 ± 0.04; Day 7: 1.42 ± 0.15; Day 10: 1.33 ± 0.10; Day 14: 1.37 ± 0.18				

the change of environmental conditions. Specifically, as the scaffolds constituents were released and the cells adapted to their environments, they may have transitioned from "survival mode" (day 1 to day 3) to proliferative phase by day 5 [35,45].

An equivalent behavior has been confirmed by Han et al., that employed OCP as filling material. Results pointed out that, although a continuously increasing cell proliferation occurs up to 6 days, OD values were lower than those of controls. The authors underlined that the reported outcomes could be misleading, due to the hydrophilic nature of SF and SF/OCP scaffolds, which could influence dye absorbance [45].

In contrast, Shao et al., found that SF scaffolds loaded with 10% HAp exhibited greater cytocompatibility than scaffolds composed of only SF, showing a sharper proliferative trend, highlighting the role of HAp in promoting bone cell adhesion and proliferation [34].

Several groups employed PicoGreen test to quantify the amount of double-stranded DNA as a marker of cell proliferation. Yan et al., experimental outputs corroborated the results obtained by other studies despite the different cellular model employed (hASCs). The DNA content of hASCs cultured on control group and SF scaffolds loaded with 16% of CaP, were similar. Specifically, the results demonstrated a sharp increase in cellular proliferation after 3 days, followed by a gradual and constant growth up to the 14th day and with no statistical differences among the groups.

The result has been confirmed by Alamar blue assay that, after a remarkable increase during the first phase of the experiments, the percentage reduction of Alamar blue reached a plateau from day 7 to day 14, underlining a non-cytotoxic behavior of the neat and composite scaffolds, as well as growing support substrate in the regard of hASCs [32].

The same considerations may be drawn for the results produced by Pina et al. that employed the same cellular model but a different ceramic filler material (β-TCP), with a concentration of 30% wt/wt [30].

The authors demonstrated a comparable amount of DNA between the SF and SF/β-TCP scaffolds at the same time intervals considered by Yan et al., but interestingly showing a proliferation increase six times greater than control at day 28 (0.06 ± 0.002 μg/ml vs. 0.01 ± 0.003 μg/ml). In contrast, the Alamar Blue assay revealed a significant difference in cell viability between the control group and the β-TCP-loaded scaffold, with the latter showing consistently higher viability across all time points and peaking at day 14, highlighting the supportive role of calcium-based materials in promoting cell viability.

Huang et al. tested 3D composite scaffolds made of SF/HAp, prepared by freeze drying of an aqueous silk solution with irregular HAp aggregates and HAp/silk nanoparticles homogenously dispersed in, at two weight contents (*i.e.* 20% and 40%). DNA quantification reveled that cell number increased up to 12 days without reaching a plateau for all the analyzed structures. Scaffolds incorporating 40% hydroxyapatite nanoparticles exhibited the highest values, followed by those containing 40% HAp aggregates, 20% HAp nanoparticles, and 20% HAp aggregates. In contrast, pure SF scaffolds demonstrated the lowest values. This peculiar behavior has been attributed to the homogeneous distribution of HAp nanoparticles inside the silk matrix, providing a more suitable microenvironment for BMSCs proliferation [33].

Notably, Lee et al. emphasized the predominant role of the polymeric matrix in promoting cellular activity over the inorganic component. Specifically, although an overall increase in BMSC proliferation was observed throughout the culture period, the results consistently demonstrated that the SF matrix provided a more favorable environment for BMSC proliferation compared to scaffolds containing increasing concentrations of β-TCP at 25%, 50%, and 75% [42].

3.5.1.2. Osteogenic differentiation. Osteogenic differentiation is a critical step that 3D scaffolds for bone tissue engineering applications should support to favor new bone matrix deposition and mineralization as it affects graft's clinical performance.

Table 5
In vivo results obtained across studies included in the systematic review. Data includes new bone formation (%), percentage of bone volume/total volume (% BV/TV), bone mineral density (g/cm^3) for the control and intervention groups. Abbreviations employed: Silk Fibroin (SF); Octacalcium Phosphate (OCP); β -Tricalcium Phosphate (β-TCP); Hydroxyapatite (HA or Hap or HAP); Nano-hydroxyapatite (nHAp); Polydopamine (PDA); Oxidized silk fibroin (OxSF); Amorphous Calcium Phosphate (ACP); Platelet-Rich-Plasma (PRP); Not applicable (N.A.).

First author and Year	Species; animal sex; age	Experimental model; bone defect size; experimental time points	New bone formation (%)				Percentage Bone Volume (% BV/TV)				Bone Mineral Density (g/cm^3)				Main *in vivo* outcomes
			Control Group	Intervention Group 1	Intervention Group 2	Intervention Group 3	Control Group	Intervention Group 1	Intervention Group 2	Intervention Group 3	Control Group	Intervention Group 1	Intervention Group 2	Intervention Group 3	
Han F. et al., 2019	Sprague-Dawley rats; male; N. A.	Calvaria defect; circular defect φ 5 mm; 12 weeks	N.A.	N.A.	N.A.	N.A.	3.62 ± 0.66 %	SF/OCP 7.87 ± 3.98 %	N.A.	N.A.	N.A.	N.A.	N.A.	N.A.	SF/OCP scaffolds showed superior integration at the interface with natural bone compared to SF scaffolds. Moreover, new bone tissue is observed in the central part of the scaffold, not only around the perimeter.
Jing T. et al., 2022	New Zeland Rabbits; male; 3 months	Calvaria defect; circular defect φ 8 mm and thickness 4 mm; 4–12 weeks	N.A.	N.A.	N.A.	N.A.	4 weeks: 16.22 ± 2.31%; 12 weeks: 23.11 ± 2.39%;	4 weeks: 20.86 ± 2.62%; 12 weeks: 38.89 ± 5.09%	Silk Fibroin/ b-Tricalcium Phosphate 2:1 4 weeks: 29.45 ± 5.32%; 12 weeks: 47.12 ± 6.55%	Silk Fibroin/ b-Tricalcium Phosphate 1:1 4 weeks: 38.45 ± 3.08%; 12 weeks: 69.31 ± 4.62%	N.A.	N.A.	N.A.	N.A.	All the scaffolds loaded with β-TCP showed an improved osteoregeneration *in vivo*. Among the groups, SF/β-TCP (1/2) favored a better initial bone formation as well as an improved bone maturation
Ko E. et al., 2017	BALB/c-nu mouse; N.A.; N.A.	Calvaria defect; circular defect φ 4 mm; 8 weeks	SF (no cells): 48.13 ± 26.74; SF (hADMSC): 52.39 ± 17.68; SF(TAZ-hADMSC): 56.86 ± 17.26	SF/Hap (no cells): 49.57 ± 19.37 SF/Hap (hADMSC): 70.67 ± 28.63 SF/Hap (TAZ-hADMSC): 87.57 ± 4.42	Hap-PDA-SF/Hap (no cells): 80.49 ± 24.21; Hap-PDA-SF/Hap (hADMSC): 97.81 ± 3.16; Hap-PDA-SF/Hap (TAZ-hADMSC): 98.06 ± 0.84	N.A.	SF (no cells): 15.88 ± 6.24; SF (hADMSC): 21.173 ± 5.68; SF(TAZ-hADMSC): 31.04 ± 7.04	SF/Hap (no cells): 18.16 ± 0.96 SF/Hap (hADMSC): 22 ± 3.52; SF/Hap (TAZ-hADMSC): 48.19 ± 0.00	Hap-PDA-SF/Hap (no cells): 33.68 ± 8; Hap-PDA-SF/Hap (hADMSC): 42.96 ± 10.32; Hap-PDA-SF/Hap (TAZ-hADMSC): 57.12 ± 4.88	N.A.	N.A.	N.A.	N.A.	N.A.	Electrospun SF nanofibrous scaffolds engineered with two-stage HAp incorporation in both inner portions and outer surfaces of the nanofiber structures promoted hADMSC osteogenesis *in vitro* and mineralized bone formation *in vivo*. Moreover, genetic engineering of hADMSCs with pTAZ plasmid further potentiated the osteoconductive capacity of the engineered SF

(*continued on next page*)

Table 5 (*continued*)

First author and Year	Species; animal sex; age	Experimental model; bone defect size; experimental time points	New bone formation (%)				Percentage Bone Volume (% BV/TV)				Bone Mineral Density (g/cm^3)				Main *in vivo* outcomes
			Control Group	Intervention Group 1	Intervention Group 2	Intervention Group 3	Control Group	Intervention Group 1	Intervention Group 2	Intervention Group 3	Control Group	Intervention Group 1	Intervention Group 2	Intervention Group 3	
															scaffolds with two-stage HAp modification.
Lee D. et al., 2017	Sprague Dawley rats; female; 1.5 months	Calvaria defect; rectangular 5 × 4mm; 2-4-8 weeks	N.A.	N.A.	N.A.	N.A.	SF100: 2 weeks: 39.15 ± 2.60%; 4 weeks: 45.51 ± 1.59%; 8 weeks: 45.83 ± 0.85%	SF75/β-TCP 25: 2 weeks: 60.21 ± 2.65%; 4 weeks: 70.92 ± 0.95%; 8 weeks; 75.58 ± 1.06%	SF50/β-TCP 50: 2 weeks: 31.70 ± 0.16%; 4 weeks: 41.77 ± 0.42%; 8 weeks: 52.33 ± 0.37%	SF25/β-TCP 75: 2 weeks: 24.56 ± 1.91%; 4 weeks: 50.67 ± 0.9%; 8 weeks: 58.91 ± 2.54%	SF100: 2 weeks: 0.24 ± 0.00 g/cm^3; 4 weeks: 0.34 ± 0.02 g/cm^3; 8 weeks: 0.37 ± 0.01 g/cm^3	SF75/β-TCP 25: 2 weeks: 0.38 ± 0.00 g/cm^3; 4 weeks: 0.53 ± 0.01 g/cm^3; 8 weeks: 0.63 ± 0.01 g/cm^3	SF50/β-TCP 50: 2 weeks: 0.11 ± 0.00 g/cm^3; 4 weeks: 0.32 ± 0.00 g/cm^3; 8 weeks: 0.42 ± 0.02 g/cm^3	SF75/β-TCP 25: 2 weeks: 0.07 ± 0.00 g/cm^3; 4 weeks: 0.34 ± 0.00 g/cm^3; 8 weeks: 0.49 ± 0.02 g/cm^3	SF/β-TCP scaffolds supported bone development, with SF75/β-TCP25 specifically promoting bone mineralization, tissue formation, and collagen production.
Liu H. et al., 2015	Sprague-Dawley rats; Male/ Female; 2 months	Calvaria defect; bilateral full-thickness quadrate defects of 5 mm × 5 mm; 8–16 weeks	* 8 weeks: 1.16 ± 0.20; 16 weeks: 1.70 ± 0.18	SF-nHAp * 8 weeks: 1.63 ± 0.23; 16 weeks: 2.44 ± 0.47	N.A.	N.A.	N.A.	N.A.	N.A.	N.A.	N.A.	N.A.	N.A.	N.A.	SF-nHAp scaffolds showed an enhanced bone-regenerative capacity compared to SF scaffolds in cranial bone defect models
Park J. Y. et al., 2015	New Zealand White Rabbits; Male; 4–5 months	Calvaria defect; circular defect φ 8 mm; 2–4 weeks	2 weeks: 0.4 ± 0.13 mm^2; 4 weeks: 1.36 ± 0.47 mm^2	PDLSS 2 weeks: 0.7 ± 0.5 mm2; 4 weeks: 0.54 ± 1.23 mm2	DPSS 2 weeks: 0.84 ± 0.93 mm2 4 weeks: 0.67 ± 0.39 mm2	N.A.	N.A.	N.A.	N.A.	N.A.	N.A.	N.A.	N.A.	N.A.	nHA-coated silk fibroin scaffolds had a great biocompatibility, promoted the formation of superficial blood vessel network after 4 weeks as well as a completely resolution of the inflammation process. Induced a slight formation of new bone. The addition of hPDLCs and hDPCs did not show a significant early effect on bone augmentation.
Park H. J. et al., 2016	Sprague-Dawley rats; N.A.; 2 months	Calvaria defect; circular defect φ 4 mm and thickness 5 mm; 1-4-8 weeks	N.A.	N.A.	N.A.	N.A.	N.A.	N.A.	N.A.	N.A.	N.A.	N.A.	N.A.	N.A.	After 8 weeks post-implantation, the SF/β-TCP scaffolds group show a faster bone regeneration SF group.

(*continued on next page*)

Table 5 (*continued*)

First author and Year	Species; animal sex; age	Experimental model; bone defect size; experimental time points	New bone formation (%)				Percentage Bone Volume (% BV/TV)				Bone Mineral Density (g/cm^3)				Main *in vivo* outcomes
			Control Group	Intervention Group 1	Intervention Group 2	Intervention Group 3	Control Group	Intervention Group 1	Intervention Group 2	Intervention Group 3	Control Group	Intervention Group 1	Intervention Group 2	Intervention Group 3	
Tang Z. et al., 2024	C57BL/6 mice; male; 7–8 weeks	Parietal bone defect; circular defect φ 5 mm; 8 weeks	N.A.	N.A.	N.A.	N.A.	26.02 ± 5.83	HA 39.45 ± 7.47	N.A.	N.A.	N.A.	N.A.	N.A.	N.A.	The nanofiber scaffolds loaded with nHA displayed a higher BV/TV compared to the group without nHA.
Yu X. et al., 2021	Sprang-Dawley rats; male; N. A.	L6 vertebral defect; hemispheric defect φ 3 mm; months (M) 1-2-3-4	N.A.	N.A.	N.A.	N.A.	M1: 0.59 ± 0.00%; M2: 0.60 ± 0.03%; M3: 0.65 ± 0.02%; M4: 0.63 ± 0.06%	nHA/SF M1: 0.64 ± 0.03%; M2: 0.58 ± 0.06%; M3: 0.65 ± 0.01%; M4: 0.69 ± 0.06	N.A.	N.A.	M1: 0.19 ± 0.04 mg/cm^3; M2: 0.18 ± 0.02 mg/cm^3; M3: 0.21 ± 0.02 mg/cm^3; M4: 0.24 ± 0.05 mg/cm^3	nHA/SF M1: 0.20 ± 0.03 mg/cm^3; M2: 0.19 ± 0.02 mg/cm^3; M3: 0.24 ± 0.02 mg/cm^3; M4: 0.27 ± 0.03 mg/cm^3	N.A.	N.A.	New bone formation extended from the edge to the center of the bone defect with a higher bone content at 12 and 16 weeks compared to 4 and 8 weeks. Bone regeneration rate was higher at nHA/SF than neat SF scaffolds
Zhu Y. et al., 2024	Sprague-Dawley rats; N.A.; N.A.	Calvaria defect; circular defect φ 5 mm; 2-8-12 weeks	12 weeks: 5.13 ± 2.67 %	OxSF 12 weeks: 12.32 ± 1.73 %	OxSF/ACP 12 weeks: 17.35 ± 3.56 %	OxSF/ACP/PRP 12 weeks: 35.40 ± 4.96 %	8 weeks: 29.93 ± 1.10 %; 12 weeks: 28.91 ± 5.56%	OxSF 8 weeks: 32.11 ± 1.38%; 12 weeks: 39.9 ± 0.79%	OxSF/ACP 8 weeks: 39.65 ± 6.27%; 12 weeks: 46. 01 ± 2.66%	OxSF/ACP/PRP 8 weeks: 55.18 ± 0.8%; 12 weeks: 57.73 ± 1.262%	8 weeks: 123.23 ± 21.58 mgHA/cc; 14 weeks: 228.17 ± 29.87 mgHA/cc	OxSF 8 weeks: 139.90 ± 50.68 mgHA/cc; 14 weeks: 318.47 ± 50.65 mgHA/cc	OxSF/ACP 8 weeks: 204.07 ± 23.12 mgHA/cc; 14 weeks: 321.77 ± 36.36 mgHA/cc	OxSF/ACP/PRP 8 weeks: 291.89 ± 81.72 mgHA/cc; 14 weeks: 414.68 ± 5.85 mgHA/cc	Different composite hydrogels showed different biomineralization capacities at the early stage of bone repair. Seedbed hydrogel sensibly improved and accelerated the bone repair process and early-stage vascularization. SF, OxSF and OxSF/ACP showed a reduced bone formation

In the proposed systematic review, this fundamental feature has been mainly evaluated (as reported in Table 4) through three analyses.

- Alkaline phosphatase (ALP) activity: an early osteogenic marker linked to extracellular matrix (ECM) deposition [23,30,31,33,36,38,39,42,44].
- Calcium deposition: a late marker of scaffold's capacity to induce mineralization [33,36].
- Osteogenic marker expression involved in osteoblasts differentiation and ECM synthesis (*i.e.* RUNX-2, osteocalcin (OCN), collagen type I (COL1), and bone morphogenic protein 2 (BMP-2) [23,31,33,41,42].

ALP has a pivotal role in bone formation, as this enzyme is implied in skeletal mineralization by hydrolyzing pyrophosphate to produce inorganic phosphate, fundamental to promote bone mineralization [36].

Kim et al., demonstrated that relatively low concentrations of HAp (1%, 2% and 3%) embedded in a SF hydrogel matrix, were sufficient to improve ALP activity. In detail, a 2% concentration of HAp is the minimum amount needed to significantly increase hMSCs ALP activity levels if compared to neat SF scaffolds (3.07 ± 0,39 *vs.* 1.50 ± 0.64 nmol/30 min/mg), while no significant differences were found in the samples loaded with 2% and 3% of HAp nanoparticles [39]. The same results have been obtained by Liu et al., which performed the analysis utilizing rat BMSCs; even if the authors did not provide the concentration employed in the scaffold fabrication, interestingly, it seems that the structure's stiffness did not affected the activity of ALP [39].

A different source of ceramic material has been employed by Jing et al. and Pina et al. that evaluated ALP activity for 3, 7, 14 and only 14 days, respectively. In the first case, the enzyme activity increased in all the selected groups until day 7, which was followed by a slight decrease at day 14 [30,44]. 3D structures with a β-TCP/SF ratio of 2/1 displayed a significantly higher ATP level than scaffolds loaded with β-TCP/SF 1/1 and 1/2 at day 7. No significant differences among the samples were observed at day 14. The osteogenic role of β-TCP has been also confirmed by the analysis of COL-1 expression performed by RT-PCR. Despite the absence of statistical differences among the three β-TCP scaffolds, a clear difference in COL-1 levels might be appreciated once compared to control group [44]. Moreover, in the second scenario, TCP positively influenced ALP activity compared to control, but the authors mainly underlined the role of ionic doped particles, specifically Mg, in influencing osteogenic improvements. Worth to underline that these considerations are related to hASCs cultured in a non-osteogenic medium, a clear signal of the β-TCP involvement in hASC maturation to mature osteoblastic phenotype. The same pattern for ALP activity is also valid for hASCs cultured into an osteogenic medium which displayed a doubled signal compared to the same sample cultured in a non-osteogenic medium (ALP activity normalized to DNA content: 1.23 ± 0.10 *vs.* 0.65 ± 0.04). In this case the effect might be probably due to the combination of osteogenic factors, β-TCP and ionic doped particles.

Additive components as SPI and/or GO nanoparticles, once combined with β-TCP, have demonstrated a synergistic effect on enhancing ALP activity, specifically at day 5. SF/SPI/GO/β-TCP scaffolds showed the highest level of enzyme activity with a doubled value compared to the same sample with β-TCP, hence underlining the central role of β-TCP in providing calcium and phosphate ions able to stimulate osteogenic differentiation. Moreover, a decrease and a stabilization of ALP activity levels on the 7th day are coherent with the natural osteogenic differentiation process.

The expression of markers related to osteogenesis regulation as RUNX-2, COL-1 and OCN has been performed through RT-PCR at days 7 and 14. Expression levels of RUNX-2, a key transcription factor involved in early osteogenesis, were initially lower in β-TCP-loaded scaffolds compared to the SF/SPI/GO group at day 7. However, a progressive upregulation was observed in the β-TCP group over time, ultimately exceeding the expression levels recorded in the other experimental conditions. The expression of COL-1, the primary extracellular matrix protein involved in bone tissue composition, displayed an increasing in mRNA secretion on SF/SPI, SF/SPI/β-TCP, and SF/SPI/GO/β-TCP scaffolds after 7 days, followed by a higher expression on the latter sample at day 14, significantly exceeding the other groups.

The same sample exhibited the highest peak of expression at day 7, while a progressive increase in expression was observed in the other groups. However, in contrast to earlier observations, the scaffold incorporating SPI and GO as additive components showed the highest levels of OCN expression. These findings suggest that, although OCN is typically considered a late-stage osteogenic marker, its expression may be stimulated at earlier stages under specific scaffold compositions.

Lee et al., analyzed gene expression on composite scaffolds characterized by increasing concentrations of β-TCP (25, 50 and 75%), up to 28 days. ALP activity followed the same tendency of MTT results, displaying a more marked ALP activity on SF scaffolds compared to β-TCP loaded scaffolds. Among samples loaded with the calcium-based materials, the scaffolds with SF75/β-TCP25 showed a slighter increase of ALP activity compared to the other SF/β-TCP groups. As a general matter, ALP activity tended to decrease as the concentrations of β-TCP increased. Interestingly, the SF25/β-TCP75 group showed the lowest value across all markers, indicating that β-TCP content exceeding a certain threshold might inhibit osteogenic activity. The osteogenic effect of the scaffolds loaded with the lower concentration of β-TCP (SF75/β-TCP25) was confirmed through the gene expression analysis of bone-related cytokines from BMSCs.

Specifically, the expression of OCN, COL-I and RUNX-2 was fairly higher in comparison with other SF/β-TCP scaffolds, indicating that a lower concentration of the inorganic powder could further improve the expression of cytokines implied in new bone formation.

The osteogenic features of SF/HAp composite scaffolds have been widely evaluated by other three studies that, overall, have demonstrated the pro-osteogenic role of HAp. In detail, Huang et al., underlined that osteogenic features of BMSCs can be enhanced by a uniform distribution of HAp nanoparticles dispersed within the SF matrix, as the nanometer scale favors a better cell differentiation. This aspect is confirmed by ALP activity that enhances with HAp contents increasing, but also when HAp aggregates are replaced with nanoparticles. The central role of HAp nanoparticles has been observed by evaluating the calcium content. A steady increase in calcium content is observed on SF/HAp scaffolds, indicating an enhanced mineralization, with a higher concentration on HAp loaded samples. Interestingly after 28 days, the calcium content is significantly higher in composite scaffolds containing HAp nanoparticles [33]. From a molecular point of view, such data are confirmed by the analysis of osteogenic markers expression through RT-PCR. The expression of RUNX-2, an early marker of osteogenic maturation, is highest at day 7 on all the composite scaffolds containing HAp nanoparticles. Moreover, osteocalcin levels increase over time, with higher expression on scaffolds containing 40% of HAp nanoparticles, thus underlining their role in osteogenic maturation.

The role of HAp has been also evaluated by Kim et al., that combined HA and TiO_2, showing that the addition of HAp was sufficient to improve osteogenic response in terms of ALP activity, which almost tripled its value at day 14 compared to SF control (0.546 ± 0.04 *vs.* 0.192 ± 0,02); nevertheless, the porous SF/TiO_2/HAp hybrid scaffolds show a significantly higher ALP activity after 7 and 14 days of cultures compared to SF pristine scaffolds. The expression levels of OCN, COL-1, and RUNX-2 mRNA were higher on the SF/TiO_2/HAp hybrid scaffold, at 14 days, as well as SF/HAp hybrid scaffold, if compared with SF neat scaffold.

3.5.2. *In vivo biological testing*

To validate the biological benefits of calcium-based materials incorporated into a SF matrix, composite scaffolds have also been evaluated in preclinical *in vivo* studies (detailed in Fig. 3), with the corresponding results presented in Table 5. Six records utilized Sprague Dawley rats as animal model [39–43,45], two records made use of New

Zealand white rabbits [37,44], one record amployed BALB/c-nu mouse [46] and the last selected one used C57BL/6 mouse [38].

The population age of the experimental animals varied from 1.5 months [42] to 4–5 months [37]. Eight records out of ten designed calvaria defects [37,39,40,42,43,45,46], while the remaining two performed a parietal bone and L6 vertebral defects, respectively [38,41]. The defects size ranged from a minimum of 3 mm in diameter [41] to a maximum of 8 mm [37,44]. The majority of the analyzed studies employed a circular defect of 5 mm in diameter [38,40,43,45], with the exception of a record showing a 4 mm circular defect [46] and one employing a bilateral full-thickness square defect of 5 mm × 5 mm [39].

The selection of experimental time points in the *in vivo* studies is crucial for assessing the biological response, encompassing early-stage tissue reaction, mid-term bone regeneration, and long-term material integration and degradation. Accordingly, the time points varied across the different studies. Only one record proposed an early stage evaluation after 1 week on scaffold's placement [43], while three studies started the analysis after 2 weeks [37,40,42], other two of them after 4 weeks [41,44] and three studies have analyzed tissue response to scaffolds positioning at the target site after 8 weeks [38,39,46]. Among them, Ko et al. and Tang et al., have analyzed a single time point [38,46] while Liu et al., performed the analysis again after 16 weeks [39]. The latter, together with the study performed by Yu et al. shows an analysis carried out on the longest time scale [41]. Three records assessed scaffold integration after 12 weeks as last experimental time point [40,44,45].

Regenerative outcomes for 3D structures have been mainly evaluated through the assessment of bone formation, percentage of bone volume (BV/TV) and Bone Mineral Density (BMD).

Quantitative analysis demonstrated that the loading of calcium-based materials (*i.e.* nHAp, β-TCP, OCP and ACP) positively affected new bone formation, due to their osteoconductive properties and similarity to bone's inorganic phase. Liu et al., and Yu et al. both utilized nHAp-SF composites, demonstrating enhanced bone regeneration in calvaria defects and vertebral defects, respectively. Specifically, the first study demonstrated that bone-like structures filled the defects area for more than the 50% of the total volume at 16 weeks post implantation, showing the central role of composite structures against SF scaffolds (2.44 ± 0.47 *vs.* 1.70 ± 0.20 relative IOD) [39]. The reported results are supported by the second study, which highlighted an increase in the percentage of bone volume between the SF and SF-nHAP scaffods after 16 weeks (0.63 ± 0.06% *vs.* 0.70 ± 0.06%) [41].

Remarkably, Ko et al. further enhanced osteogenic potential through the incorporation of nHAp by means of a two-stage process, consisting on a first incorporation of HAp during the electrospinning process followed by a second immobilization via PDA-mediated adhesive chemistry, which brought to an improvement of mechanical and osteoconductive properties. Indeed, after 8 weeks, nHAp-containing SF scaffold (SF/HAp) did not show any sensitive increase of bone regeneration compared to SF control (49.57 ± 19.37% *vs.* 48.13 ± 26.74%), HAp-PDA-SF/HAp scaffolds, leads to a in increment of bone regeneration of 62.28% and 67.27% compared to control and SF/HAp groups (80.49 ± 24.21%). This results were also confirmed by BV/TV quantification [46].

The central role of nHAp in osteogenic enhancement has been also validated by Park et al. by exploring the use nHAp as a coating material. Herein, the role of dental pulp (DPSS) and periodontal ligament-derived cells (PDLSS) in bone regeneration has been studied, suggesting that the biological functionalization with DPSS and PDLSS did not show a significant early effect on bone augmentations in the selected animal model, which can be attributed to the coating with nHAp [37].

β-TCP has been shown to play a crucial role in promoting osteogenesis *in vivo*. Clearly, the β-TCP concentration is fundamental to obtain an improved *in vivo* outcome. In this light, Lee et al. analyzed the role of increasing concentrations of β-TCP embodied in SF matrix (0, 25, 50 and 75%). New bones were considerably formed in defects filled with scaffolds loaded with 25% of β-TCP. Specifically, after only two weeks from the implantation, this scaffold induced a sensible increase of BV/TV compared to the other samples (60.21 ± 2.65% *vs.* 39.15 ± 2.60%, 31.67 ± 0.16%, 24.56 ± 1.91%, for SF100, SF50/β-TCP50 and SF25/β-TCP75, respectively). This pattern has been further confirmed after 8 weeks, with BV/TV values of 75.58 ± 1.06% *vs.* 45.83 ± 0.85%, 52.33 ± 0.37%, 58.91 ± 2.54% for SF100, SF50/β-TCP50 and SF25/β-TCP75, respectively. Moreover, SF75/β-TCP25 scaffold showed higher BMD than the other defects. In conclusion the central role of 25% β-TCP concentration compared to the other tested amounts of the mineral component has been proved also for bone volume, bone surface, trabecular number and trabecular separation [42].

Interestingly, Jing et al. who evaluated half, equal and double concentrations of β-TCP relative to SF amount reported different findings. In particular, they demonstrated that the scaffolds loaded with twice β-TCP concentration, termed SF/β-TCP (1/2), displayed the highest bone formation capacity, covering two-thirds of the defect area after 12 weeks. Moreover, in terms of BV/TV, as SF scaffolds showed a gradual but slower increase over time, β-TCP loaded structures exhibited significantly higher values than those at 4 weeks. Notably, SF/β-TCP(1/2) scaffolds achieved a significant higher BV/TV level compared to the other groups. However, it is worthy to note that *in vivo* studies were conducted in two different animal models (Sprangue-Dawley Rats and New Zealand White Rabbits) indicating that bone regenerative patterns might be also correlated to the different animal species [44].

Park et al. investigated the role of β-TCP particle size on bone regeneration, utilizing two size ranges: 300–600 μm (GS) and 600–900 μm (GM). Their findings consistently showed that while SF/β-TCP scaffolds enhanced bone regeneration compared to pristine SF scaffolds, particle size did not significantly affect the regenerative process. This suggests that the observed regeneration outcomes can be primarily attributed to the intrinsic properties of β-TCP rather than its particle size [43].

Finally, two studies employed OCP, a mineral precursor to carbonate-containing calcium-deficient hydroxyapatite and ACP as alternative calcium-sources [40,45].

As a result, compared to SF scaffolds OCP exhibited good bone forming abilities, demonstrating superior integration at the interfaces with natural bone (3.62 ± 0.66% *vs.* 7.87 ± 3.98% BV/TV). In addition, new bone formation has been observed also in the central part of SF/OCP scaffolds, highlighting how the synergistic coupling of degradative materials properties and an appropriate porosity, may facilitate cell ingrowth. In fact, OCP can be resorbed by osteoclasts, leaving void spaces that may further support cellular infiltration and tissue regeneration.

Similarly, oxidized SF scaffolds combined with amorphous calcium phosphate (OxSF/ACP) and PRP exhibited the highest bone regeneration at 12 weeks (35.40 ± 4.96%) compared to that allowed by pure SF scaffolds (5.13 ± 2.67%), along with a noticeable increase of BV/TV (57.73 ± 1.26 *vs.* % 23.11 ± 2.39%). These findings reinforce the notion that hydrogels significantly enhance and accelerate bone repair process, possibly as a consequence of mineralization capacity and promotion of early-stage vascularization.

4. Discussion

This systematic review investigates the potential of SF three-dimensional scaffolds enriched with calcium-based material for applications related to bone tissue regeneration. The analysis of the 19 selected studies reveals compelling evidence that the incorporation of an inorganic phase, primarily nHAp, β-TCP, OCP and ACP, markedly enhances the mechanical and biological properties of SF-based scaffolds, both *in vitro* and *in vivo* preclinical studies.

It is widely recognized that synthetic bone grafts must meet stringent morphological and structural requirements, including an interconnected porous architecture that closely mimics the mineralized extracellular matrix of native bone tissue, as these features are fundamental for the

future development of personalized technologies in regenerative medicine, such as patient-specific 3D-printed scaffolds enabling improved tissue integration and functional recovery [51,52]. In this perspective, recent advances in biomaterials design increasingly emphasize the importance of biomimicry and multiscale structural organization, arguing that effective bone regeneration relies on scaffolds capable of reproducing the hierarchical architecture of bone from the nano-to the macro-scale while simultaneously providing dynamic biological signaling through the integration of structural (*e.g.* pore size gradients and trabecular-like architectures), mechanical (*e.g.* stiffness matching and mechanotransduction), chemical (*e.g.* controlled calcium phosphate ion release and responsiveness to pH variations), and biological cues (*e.g.* growth factor delivery, extracellular matrix motif recognition, and enzymatic activity) [51]. Building on this paradigm, one of the most relevant future directions concerns the development of multi-responsive SF–based smart scaffolds capable of dynamically adapting to the evolving bone healing microenvironment [53]. While current systems predominantly rely on passive ion release and static architectures, emerging strategies aim to engineer scaffolds that actively respond to biological stimuli such as enzymatic activity, local pH changes, inflammatory signals, and mechanical loading [54]. In this context, the intrinsic tunability of SF crystallinity and degradation kinetics offers a unique opportunity to synchronize scaffold resorption with new bone formation, thereby enhancing the temporal and functional coordination between material degradation and tissue regeneration. Additionally, the ideal scaffolds should present bioactive sites capable of supporting cellular adhesion, proliferation, and subsequent tissue regeneration, as well as enabling controlled release of bioactive molecules and promoting stem cell differentiation [55]. In this respect, it is evident how scaffold's fabrication methods may play a critical role in determining the right compromise between a final structure well-mimicking the bone features (*e.g.* pore size, trabecular thickness) and a proper function in promoting bone replacement, assisted by the incorporation of growth factors.

The easy processability of SF allows the execution of various successful synthesis techniques for the fabrication of composite materials suitable for personalized bone regeneration. For instance, electrospinning is extensively used to fabricate nanostructured fibrous scaffolds that closely mimick the morphology of the ECM [56]. Neverthelsess, this method often results in reduced pore size (*i.e.* 28.3 μm as reported by Tang et al.) expected to limiting a deeper cell infiltration and vascularization [38]. Electrospun materials, given their conformation/internal structure and brittleness tendency, are not perfectly suited to applications requiring additional mechanical properties for the grafts, as in case of alveolar bone regeneration. Conversely, solvent casting particle leaching offers greater control of macroporosity, producing pore diameters ranging from 270 μm up to 700 μm, hence permitting the creation a favorable environment able to support nutrient diffusion, vascular ingrowth and bone matrix deposition. Clearly, the pore dimension is strictly dependent from the porogen employed (*e.g.* sugar, glucose, paraffin, gelatin, and ammonium chloride). This method demonstrates promising regenerative outcomes as it allows the manufacturing of 3D scaffolds better mimicking the anatomy of cancellous bone than it is done by nanofiber-based constructs [57,58].

However, a “middle ground” in the production of structures with medium porosity and employed in most of the analyzed studies is represented by freeze-drying, alone or coupled with salt-leaching or crosslinking techniques. The produced scaffolds reported moderate to high porosity (up to 92.63%) with pore size ranging from 100 μm to 300 μm, still remaining an ideal option for cell infiltration and nutrient exchange. In this light, Shao et al., compared scaffolds prepared via a conventional freeze-drying method and electrical field-induced gel, revealing that in the first case the 3D structures were characterized by a uniform disordered porous architecture while, the second production method allowed the formation of a multilevel pore size distribution with two distinct levels of pore structures wherein macropores are related to micropores [34]. Specifically has been noted that as HAp content incresead also the number of large macropores gradually augmented. Given this, freeze-drying has been recently employed by Li et al. to further improve pre-fabricated 3D structures by blending with carbodiimide-activated SF solution that, after liquid nitrogen freezing and lyophilization, allowed the formation of micro/nanofibrous pattern inside scaffold's pore spaces, hence providing topographic cues able to facilitate cell-biomaterial interactions [28,59]. Analyzing the mechanical properties of scaffolds fabricated through salt leaching/freezedrying combined technique, Pina et al. showed a SF/β-TCP composite scaffold with the highest compression modulus/strength among the ones analyzed in this review [30]. This clearly highlights how a correct use of hybrid techniques can produce SF based materials that, while maintaining a high porosity, are mechanically robust to support bone tissue formation.

The development of scaffolds with enhanced functional properties, enabled by the biomimicry of native tissue architecture and suitable for a wide range of biomedical applications, can be achieved through the use of composite biomaterials that integrate SF with inorganic components. Among them, calcium-based elements (*e.g.* nHAp, β-TCP, OCP ACP), usually in the form of nanoparticles, are largely employed for bone tissue engineering applications. Nevertheless, despite of a clear improvement of mechanical properties, balancing the amount of the ceramic component is essential to avoid the formation of excessively small pores which could negatively affect cell-cell interaction, cell migration, proliferation, adhesion and differentiation [55,60].

SF physico-chemical properties are pivotal in shaping the final scaffold's features. Indeed, porosity/pore size tunability are deeply affected by polymer solution parameters (*e.g.* concentration, viscosity, and the amount of aqueous phase dispersed in the system), hence the pore's size and amount can be further modulated by controlling polymer concentration and/or viscosity [28].

The high processability of SF provides a fine tuning and optimization of SF-based materials. Moreover, the combination with calcium-based elements can generate materials with thoroughly enhanced mechanical properties and a high regenerative potential at the bone level.

In this arena, multiple studies underlined that scaffolds enriched with calcium-based fillers positively influence cellular viability, proliferation and osteogenic differentiation, with particular regard to hMSCs and BMSCs. A plausible explanation for this behavior may lie in the presence of microscale surface irregularities introduced by the integration or coating with inorganic particles. These features not only modulate the surface micro- and nanotopography but also influence key physicochemical properties such as wettability and microporosity, ultimately enhancing cell–material interactions [61].

Even if molecular mechanisms are largely unkwown, it has been widely demonstrated that the surface chemistry determined by the presence of calcium based materials, such as nHAp, is able to trigger signalling cascade of genes involved in osteoblasts maturation as ERK/Sox9, implied in expression of osteocalcin and type I collagen, integrin-BMP/Smad, Wnt/β-catenin and TGF signalling pathways [22,50,62–64].

Regarding the latter, in 2017 Zhang et al. were the first to propose that topographical cues arising from the incorporation of TCP could drive osteogenic differentiation by modulating the structure of primary cilia [11]. Specifically, mesenchymal stem cells MSCs exhibited cilia elongation on grooved surfaces, accompanied by the recruitment of p-TGFβRII to the cilia, an essential step for the activation of downstream TGF-β signaling, which is a pathway critically involved in osteogenic differentiation.

Interestingly, the degree of osteoconductivity seems to be dependent from the amount of the inorganic phase. According to our findings, a concentration ranging from 2% to 40% wt is capable to induce a robust osteogenic behaviour [30,31,33,36]. An unexpected outcome is however given by the work by Yan et al., whereas the incorporation of 16% CaP did not result in any significant differences compared to the pristine

SF scaffold [32].

In this light, the work by Lee et al. aims to assess the most suitable weight percentage content of calcium composities allowing to obtain optimal regeneration properties [42]. Herein, SF scaffolds with β-TCP content up to 75% in weight were produced, demonstrating that the best performance was obtained by SF scaffolds loaded with 25% of β-TCP, both *in vitro* and *in vivo*.

This behavior could stem from an imbalance in the cellular homeostatic mechanisms. Shih et al. demonstrated an interesting molecular mechanisms involving the dissolution/precipitation of CaP minerals responding to the increase of Ca^{2+} or PO_4^{3-} in the surrounding environment, in order to establish equilibrium conditions [65]. Briefly, it has been demonstrated that PO_4^{3-} is internalized by cells and mithocondria, where it serves as a substrate for ATP synthesis. Once secreted and metabolized into adenosine, ATP promotes osteogenic differentiation of hMSCs via activation of the A2b adenosine receptor through autocrine and/or paracrine signalling pathways. This mechanism underlines the role of phosphate ions deriving from CaP mineral dissolution/precipation and their implication in the regard of osteoprogenitor during bone remodeling. From this perspective, it is clear that excessive release of calcium ions from high-concetration calcium-based scaffolds can unbalance intracellular calcium homeostasis, thus imparing the balance required for proper stem cell differentiation.

In vivo results futher confirmed the *in vitro* trends related to SF-based biomaterials for BTE approaches [37–46]. Most experimental models, which mainly involved calvarial defect in rodents or rabbits, displayed a positive regenerative outcome in terms of new bone formation, bone mineral density and bone volume fraction, especially in experimental scenarios that involved composite grafts with medium concentration of ceramic loading (*e.g.*, SF/β-TCP at 75/25 or 1:2 ratios) [42,44]. Nevertheless, it is worth underlining that futher *in vivo* studies, with experimental time points that extend beyond 16 weeks, are required to better translate the experimental finding into a clinical contest.

Finally, while scaffold's functionalization strategies with compounds employing natural flavonoids, SeNPs, cellular models and growth factor loaded microshperes, showed interesting regenerative potential, their clinical stability still remains uncertain due to complexity in process synthesis and reproducibility.

5. Conclusion and future perspectives

Silk fibroin-based composite scaffolds enriched with calcium-based materials represent a promising strategy for bone tissue engineering, offering a favorable balance of mechanical strength, morphological characteristics, and osteoconductive properties. The fabrication methods, along with the type and concentration of calcium-phosphate fillers, must be carefully selected, as they play a critical role in directing the regenerative response to meet specific clinical needs.

Based on currently available findings, hydroxyapatite is the most commonly used calcium-based filler, followed by β-tricalcium phosphate, at various concentrations, both demonstrating promising results *in vitro* andex.

Nevertheless, further investigations using larger animal models and load-bearing conditions are necessary to validate the effectiveness of these 3D composite scaffolds and facilitate their clinical translation into human-relevant applications.

A key insight from the literature is that CaP-based fillers are not merely passive components but act as active modulators within SF-based grafts, influencing cellular behavior and tissue outcomes. The integration of ceramic phase into a SF matrix is therefore essential to accurately replicate the physicochemical environment of the bone niche, ultimately guiding the physiological processes toward a pro-regenerative outcome. Looking toward future developments, SF–based composite scaffolds enriched with calcium-based materials offer particularly promising opportunities for next-generation biomedical applications. One of the most compelling perspectives is the integration of these composites with advanced 3D printing and biofabrication technologies, enabling the production of patient-specific, anatomically tailored implants with controlled architecture and spatial distribution of bioactive phases [52] or to develop smart biomaterials able to respond to biological stimuli, releasing therapeutic agents in a controlled manner, or dynamically adapting their properties during tissue regeneration [51].Moreover, the integration of artificial intelligence and machine learning approaches into the design and development of SF-based scaffolds might represent a transformative phase in BTE. AI-driven methodologies offer the possibility to rationally optimize scaffold architecture, composition, and functional performance by identifying complex, non-linear relationships between material parameters and biological outcomes that are difficult to resolve using conventional experimental approaches alone [66–68].

In this context, the inherent biocompatibility of SF, combined with the osteoconductive and bioactive properties of calcium-based fillers, offers a versatile platform not only for enhancing current bone tissue engineering strategies but also for progressing toward personalized, smart, and translational regenerative therapies. By integrating innovative techniques with calcium phosphate incorporation, it is possible to develop multiscale, smart scaffolds in which osteogenesis is driven by the synergistic interplay of multiple instructive cues rather than isolated factors, positioning SF–based composites as highly promising candidates for next-generation biomimetic bone scaffolds.

CRediT authorship contribution statement

Biagio Matera: Writing – original draft, Methodology, Data curation, Conceptualization. **Giuseppe De Giorgio:** Writing – original draft, Methodology, Data curation, Conceptualization. **Katia Rupel:** Writing – review & editing, Project administration, Funding acquisition, Data curation, Conceptualization. **Gianluca Turco:** Writing – review & editing, Supervision, Data curation. **Pasquale D'Angelo:** Writing – review & editing, Supervision, Project administration, Funding acquisition, Data curation, Conceptualization. **Benedetta Ghezzi:** Writing – review & editing, Project administration, Funding acquisition, Data curation, Conceptualization.

Data availability Statement

The data that support the findings of this study are available from the corresponding author upon reasonable request.

Funding sources

The present work has been funded with the PRIN project: progetti di ricerca di rilevante interesse nazionale—Bando PRIN 2022 PNRR No. P2022NC9NT CUP: D53D23016540001.

Declaration of competing interest

The authors declare that they have no known competing financial interests or personal relationships that could have appeared to influence the work reported in this paper.

Acknowledgements

The present work has been fundend with the PRIN project: progetti di ricerca di rilevante interesse nazionale—Bando 2022 PNRR No. P2022NC9NT CUP: D53D23016540001, CUP: B53D23024770001, and CUP: J53D23014280001.

Appendix A. Supplementary data

Supplementary data to this article can be found online at https://doi.org/10.1016/j.ceramint.2026.01.443.

References

[1] R. Marsell, T.A. Einhorn, The biology of fracture healing, Injury 42 (6) (2011) 551–555, https://doi.org/10.1016/j.injury.2011.03.031.

[2] R. De Pace, S. Molinari, E. Mazzoni, G. Perale, Bone regeneration: a review of current treatment strategies, J. Clin. Med. 14 (6) (2025), https://doi.org/10.3390/jcm14061838. Multidisciplinary Digital Publishing Institute (MDPI).

[3] Z. Wu, Z. Meng, Q. Wu, et al., Biomimetic and osteogenic 3D silk fibroin composite scaffolds with nano MgO and mineralized hydroxyapatite for bone regeneration, J. Tissue Eng. 11 (2020), https://doi.org/10.1177/2041731420967791.

[4] V. Campana, G. Milano, E. Pagano, et al., Bone substitutes in orthopaedic surgery: from basic science to clinical practice, J. Mater. Sci. Mater. Med. 25 (10) (2014) 2445–2461, https://doi.org/10.1007/s10856-014-5240-2.

[5] J.T.B. Ratnayake, M. Mucalo, G.J. Dias, Substituted hydroxyapatites for bone regeneration: a review of current trends, J. Biomed. Mater. Res. B Appl. Biomater. 105 (5) (2017) 1285–1299, https://doi.org/10.1002/jbm.b.33651. John Wiley and Sons Inc.

[6] J. Clavero, S. Lundgren, Ramus or Chin grafts for maxillary sinus inlay and local onlay augmentation: Comparison of donor site morbidity and complications, Clin. Implant Dent. Relat. Res. 5 (3) (2003) 154–160, https://doi.org/10.1111/j.1708-8208.2003.tb00197.x. BC Decker Inc.

[7] R. Zhao, R. Yang, P.R. Cooper, Z. Khurshid, A. Shavandi, J. Ratnayake, Bone grafts and substitutes in dentistry: a review of current trends and developments, Molecules 26 (10) (2021), https://doi.org/10.3390/molecules26103007. MDPI AG.

[8] H. Kyung, N. Kang, Management of alveolar cleft, Arch Craniofac Surg 16 (2) (2015) 49, https://doi.org/10.7181/acfs.2015.16.2.49.

[9] G. Fernandez de Grado, L. Keller, Y. Idoux-Gillet, et al., Bone substitutes: a review of their characteristics, clinical use, and perspectives for large bone defects management, J. Tissue Eng. 9 (2018), https://doi.org/10.1177/2041731418776819. SAGE Publications Ltd.

[10] R.S. Valtanen, Y.P. Yang, G.C. Gurtner, W.J. Maloney, D.W. Lowenberg, Synthetic and bone tissue engineering graft substitutes: what is the future? Injury 52 (2021) S72–S77, https://doi.org/10.1016/j.injury.2020.07.040.

[11] L. Zhang, G. Yang, B.N. Johnson, X. Jia, Three-dimensional (3D) printed scaffold and material selection for bone repair, Acta Biomater.Acta Materialia Inc. 84 (2019) 16–33, https://doi.org/10.1016/j.actbio.2018.11.039.

[12] J. Gaweł, J. Milan, J. Żebrowski, D. Płoch, I. Stefaniuk, M. Kus-Liśkiewicz, Biomaterial composed of chitosan, riboflavin, and hydroxyapatite for bone tissue regeneration, Sci. Rep. 13 (1) (2023), https://doi.org/10.1038/s41598-023-44225-0.

[13] D. Gong, Q. Zhai, M. Wu, X. Tao, F. Wang, Promotion of rat femoral distal bone defect repair using alginate-silk fibroin composite hydrogel, Int. Immunopharmacol. 161 (2025), https://doi.org/10.1016/j.intimp.2025.114973.

[14] K.M. N'Gatta, E.F. Assanvo, J. El Hayek, et al., 3D-Printed polycaprolactone scaffolds reinforced with cellulose nanocrystals and silver nanoparticles for bone tissue engineering, ACS Appl. Mater. Interfaces (2025), https://doi.org/10.1021/acsami.5c06504. Published online.

[15] Q. Zhang, Z. Liu, Y.Y. He, et al., Osteoimmunity-Regulating biospun 3D silk scaffold for bone regeneration in critical-size defects, J. Adv. Res. (2025), https://doi.org/10.1016/j.jare.2025.04.032. Published online.

[16] Y.M. Sillmann, P. Eber, E. Orbeta, F. Wilde, A.J. Gross, F.P.S. Guastaldi, Milestones in mandibular bone tissue engineering: a systematic review of large animal models and critical-sized defects, J. Clin. Med. 14 (8) (2025), https://doi.org/10.3390/jcm14082717. Multidisciplinary Digital Publishing Institute (MDPI).

[17] L.P. Yan, J.M. Oliveira, A.L. Oliveira, S.G. Caridade, J.F. Mano, R.L. Reis, Macro/microporous silk fibroin scaffolds with potential for articular cartilage and meniscus tissue engineering applications, Acta Biomater. 8 (1) (2012) 289–301, https://doi.org/10.1016/j.actbio.2011.09.037.

[18] G. De Giorgio, B. Matera, D. Vurro, et al., Silk fibroin materials: biomedical applications and perspectives, Bioengineering 11 (2) (2024), https://doi.org/10.3390/bioengineering11020167. Multidisciplinary Digital Publishing Institute (MDPI).

[19] A. Reizabal, C.M. Costa, L. Pérez-Álvarez, J.L. Vilas-Vilela, S. Lanceros-Méndez, Silk fibroin as sustainable advanced material: material properties and characteristics, processing, and applications, Adv. Funct. Mater. 33 (3) (2023), https://doi.org/10.1002/adfm.202210764. John Wiley and Sons Inc.

[20] T.P. Nguyen, Q.V. Nguyen, V.H. Nguyen, et al., Silk fibroin-based biomaterials for biomedical applications: a review. *Polymers (Basel)*, MDPI AG 11 (12) (2019), https://doi.org/10.3390/polym11121933.

[21] Y. Lin, L. Zhao, H. Jin, et al., Multifunctional applications of silk fibroin in biomedical engineering: a comprehensive review on innovations and impact, Int J Biol Macromol.Elsevier B.V. 309 (2025), https://doi.org/10.1016/j.ijbiomac.2025.143067.

[22] S. Zhu, Q. Zhang, X. Xu, et al., Recent advances in silk fibroin-based composites for bone repair applications: a review, Polymers 17 (6) (2025), https://doi.org/10.3390/polym17060772. Multidisciplinary Digital Publishing Institute (MDPI).

[23] F. Liu, C. Liu, B. Zheng, et al., Synergistic effects on incorporation of β-tricalcium phosphate and graphene oxide nanoparticles to silk fibroin/soy protein isolate scaffolds for bone tissue engineering, Polymers 12 (1) (2020), https://doi.org/10.3390/polym12010069.

[24] B. Ghezzi, B. Matera, M. Meglioli, et al., Composite PCL scaffold with 70% β-TCP as suitable structure for bone replacement, Int. Dent. J. 74 (6) (2024) 1220–1232, https://doi.org/10.1016/j.identj.2024.02.013.

[25] J.R. Vetsch, S.J. Paulsen, R. Müller, S. Hofmann, Effect of fetal bovine serum on mineralization in silk fibroin scaffolds, Acta Biomater. 13 (2015) 277–285, https://doi.org/10.1016/j.actbio.2014.11.025.

[26] B. Kundu, R. Rajkhowa, S.C. Kundu, X. Wang, Silk fibroin biomaterials for tissue regenerations, Adv. Drug Deliv. Rev. 65 (4) (2013) 457–470, https://doi.org/10.1016/j.addr.2012.09.043.

[27] W. Sun, D.A. Gregory, M.A. Tomeh, X. Zhao, Molecular sciences silk fibroin as a functional biomaterial for tissue engineering, J. Mol. Sci. 22 (2021) 1499, https://doi.org/10.3390/ijms2.

[28] L. Ma, W. Dong, E. Lai, J. Wang, Silk fibroin-based scaffolds for tissue engineering, Front. Bioeng. Biotechnol. 12 (2024), https://doi.org/10.3389/fbioe.2024.1381838. Frontiers Media SA.

[29] Huwaldt JA. Plot Digitizer, Version 2.6.11. https://plotdigitizer.sourceforge.net.

[30] S. Pina, R.F. Canadas, G. Jiménez, et al., Biofunctional ionic-doped calcium phosphates: silk fibroin composites for bone tissue engineering scaffolding, Cells Tissues Organs 204 (3–4) (2017) 150–163, https://doi.org/10.1159/000469703.

[31] J.H. Kim, D.K. Kim, O.J. Lee, et al., Osteoinductive silk fibroin/titanium dioxide/hydroxyapatite hybrid scaffold for bone tissue engineering, Int. J. Biol. Macromol. 82 (2016) 160–167, https://doi.org/10.1016/j.ijbiomac.2015.08.001.

[32] L.P. Yan, J.M. Oliveira, A.L. Oliveira, R.L. Reis, In vitro evaluation of the biological performance of macro/micro-porous silk fibroin and silk-nano calcium phosphate scaffolds, J. Biomed. Mater. Res. B Appl. Biomater. 103 (4) (2015) 888–898, https://doi.org/10.1002/jbm.b.33267.

[33] X. Huang, S. Bai, Q. Lu, X. Liu, S. Liu, H. Zhu, Osteoinductive-nanoscaled silk/HA composite scaffolds for bone tissue engineering application, J. Biomed. Mater. Res. B Appl. Biomater. 103 (7) (2015) 1402–1414, https://doi.org/10.1002/jbm.b.33323.

[34] Y.F. Shao, H. Wang, Y. Zhu, et al., Hydroxyapatite/Silk fibroin composite scaffold with a porous structure and mechanical strength similar to cancellous bone by electric field-induced gel technology, ACS Appl. Mater. Interfaces 16 (44) (2024) 60977–60991, https://doi.org/10.1021/acsami.4c12470.

[35] A. Shahid, F. Moeen, S. Habib, et al., Mg doped ZnO containing silk nanocomposite scaffolds for biofilm prevention during alveolar bone regeneration, Mater. Chem. Phys. 327 (2024), https://doi.org/10.1016/j.matchemphys.2024.129911.

[36] M.H. Kim, B.S. Kim, J. Lee, D. Cho, O.H. Kwon, W.H. Park, Silk fibroin/hydroxyapatite composite hydrogel induced by gamma-ray irradiation for bone tissue engineering, Biomater. Res. 21 (1) (2017), https://doi.org/10.1186/s40824-017-0098-2.

[37] J.Y. Park, C. Yang, I.H. Jung, et al., Regeneration of rabbit calvarial defects using cells-implanted nano-hydroxyapatite coated silk scaffolds, Biomater. Res. 19 (1) (2015), https://doi.org/10.1186/s40824-015-0027-1.

[38] Z. Tang, J. Li, L. Fu, et al., Janus silk fibroin/polycaprolactone-based scaffold with directionally aligned fibers and porous structure for bone regeneration, Int. J. Biol. Macromol. 262 (2024), https://doi.org/10.1016/j.ijbiomac.2024.129927.

[39] H. Liu, G.W. Xu, Y.F. Wang, et al., Composite scaffolds of nano-hydroxyapatite and silk fibroin enhance mesenchymal stem cell-based bone regeneration via the interleukin 1 alpha autocrine/paracrine signaling loop, Biomaterials 49 (2015) 103–112, https://doi.org/10.1016/j.biomaterials.2015.01.017.

[40] Y. Zhu, H. Gu, J. Yang, et al., An Injectable silk-based hydrogel as a novel biomineralization seedbed for critical-sized bone defect regeneration, Bioact. Mater. 35 (2024) 274–290, https://doi.org/10.1016/j.bioactmat.2024.01.024.

[41] X. Yu, G. Shen, Q. Shang, et al., A Naringin-loaded gelatin-microsphere/nano-hydroxyapatite/silk fibroin composite scaffold promoted healing of critical-size vertebral defects in ovariectomised rat, Int. J. Biol. Macromol. 193 (2021) 510–518, https://doi.org/10.1016/j.ijbiomac.2021.10.036.

[42] D.H. Lee, N. Tripathy, J.H. Shin, et al., Enhanced osteogenesis of β-tricalcium phosphate reinforced silk fibroin scaffold for bone tissue biofabrication, Int. J. Biol. Macromol. 95 (2017) 14–23, https://doi.org/10.1016/j.ijbiomac.2016.11.002.

[43] H.J. Park, K.D. Min, M.C. Lee, et al., Fabrication of 3D porous SF/β-TCP hybrid scaffolds for bone tissue reconstruction, J. Biomed. Mater. Res. 104 (7) (2016) 1779–1787, https://doi.org/10.1002/jbm.a.35711.

[44] T. Jing, liu yi, L. Xu, C. Chen, F. Liu, The incorporation of β-tricalcium phosphate nanoparticles within silk fibroin composite scaffolds for enhanced bone regeneration: an in vitro and in vivo study, J. Biomater. Appl. 36 (9) (2022) 1567–1578, https://doi.org/10.1177/08853282211065621.

[45] F. Han, Y. Hu, J. Li, et al., In situ silk fibroin-mediated crystal formation of octacalcium phosphate and its application in bone repair, Mater. Sci. Eng. C 95 (2019) 1–10, https://doi.org/10.1016/j.msec.2018.10.041.

[46] E. Ko, J.S. Lee, H. Kim, et al., Electrospun silk fibroin nanofibrous scaffolds with two-stage hydroxyapatite functionalization for enhancing the osteogenic differentiation of human adipose-derived mesenchymal stem cells. *ACS appl mater interfaces*, Am. Chem. Soc. 10 (9) (2018) 7614–7625, https://doi.org/10.1021/acsami.7b03328.

[47] R. Lyu, T. Wang, C. Li, et al., Preparation of ion-doped nano-hydroxyapatite Bombyx Mori silk fibroin composite membrane by electrochemical deposition for enhancing osteogenic differentiation in vitro and in vivo, Int. J. Biol. Macromol. 318 (2025), https://doi.org/10.1016/j.ijbiomac.2025.144603.

[48] D.N. Rockwood, R.C. Preda, T. Yücel, X. Wang, M.L. Lovett, D.L. Kaplan, Materials fabrication from Bombyx mori silk fibroin, Nat. Protoc. 6 (10) (2011) 1612–1631, https://doi.org/10.1038/nprot.2011.379.

[49] A. Ajisawa, Dissolution of Silk Fibroin with Calciumchloride/Ethanol Aqueous Solution, 1997.

[50] H. Liu, H. Peng, Y. Wu, et al., The promotion of bone regeneration by nanofibrous hydroxyapatite/chitosan scaffolds by effects on integrin-BMP/Smad signaling pathway in BMSCs, Biomaterials 34 (18) (2013) 4404–4417, https://doi.org/10.1016/j.biomaterials.2013.02.048.

[51] S.M.M. Hossen, M.A. Khaleque, M.S. Lim, et al., Biomimetic strategies for bone regeneration: smart scaffolds and multiscale cues, Biomimetics 11 (1) (2025) 12, https://doi.org/10.3390/biomimetics11010012.
[52] Q. Wang, G. Han, S. Yan, Q. Zhang, 3D printing of silk fibroin for biomedical applications, Materials.MDPI AG. 12 (3) (2019), https://doi.org/10.3390/ma12030504.
[53] A. Mushtaq, K.L. Do, A. Wahab, et al., Silk fibroin-derived smart living hydrogels for regenerative medicine and organoid engineering: bioactive, adaptive, and clinically translatable platforms, Gels 11 (11) (2025), https://doi.org/10.3390/gels11110908. Multidisciplinary Digital Publishing Institute (MDPI).
[54] P.S. Kowalski, C. Bhattacharya, S. Afewerki, R. Langer, Smart biomaterials: recent advances and future directions, ACS Biomater. Sci. Eng. 4 (11) (2018) 3809–3817, https://doi.org/10.1021/acsbiomaterials.8b00889.
[55] M. Patel, S.P. Singh, D.K. Dubey, Insights into nanomechanical behavior of B. mori silk fibroin-hydroxyapatite bio-nanocomposite using MD simulations: role of varying hydroxyapatite content, J. Mech. Behav. Biomed. Mater. 147 (2023), https://doi.org/10.1016/j.jmbbm.2023.106125.
[56] N. Chen, W. Jin, H. Gao, et al., Sequential intervention of anti-inflammatory and osteogenesis with silk fibroin coated polyethylene terephthalate artificial ligaments for anterior cruciate ligament reconstruction, J. Mater. Chem. B 11 (34) (2023) 8281–8290, https://doi.org/10.1039/d3tb00911d.
[57] M. Rajabi, M. Firouzi, Z. Hassannejad, I. Haririan, P. Zahedi, Fabrication and characterization of electrospun laminin-functionalized silk fibroin∀poly(ethylene oxide) nanofibrous scaffolds for peripheral nerve regeneration, J. Biomed. Mater. Res. B Appl. Biomater. 106 (4) (2018) 1595–1604, https://doi.org/10.1002/jbm.b.33968.
[58] H. Wu, C. Zhao, K. Lin, X. Wang, Mussel-Inspired polydopamine-based multilayered coatings for enhanced bone Formation, Front. Bioeng. Biotechnol. 10 (2022), https://doi.org/10.3389/fbioe.2022.952500. Frontiers Media S.A.
[59] Y. Li, Y. Liu, Q. Guo, Silk fibroin hydrogel scaffolds incorporated with chitosan nanoparticles repair articular cartilage defects by regulating TGF-β1 and BMP-2, Arthritis Res. Ther. 23 (1) (2021), https://doi.org/10.1186/s13075-020-02382-x.
[60] A. Zuluaga-Vélez, A. Quintero-Martinez, L.M. Orozco, J.C. Sepúlveda-Arias, Silk fibroin nanocomposites as tissue engineering scaffolds – a systematic review, Biomed. Pharmacother. (2021) 141, https://doi.org/10.1016/j.biopha.2021.111924. Elsevier Masson s.r.l.
[61] B. Ghezzi, P. Lagonegro, N. Fukata, et al., Sub-micropillar spacing modulates the spatial arrangement of mouse mc3t3-e1 osteoblastic cells, Nanomaterials 9 (12) (2019), https://doi.org/10.3390/nano9121701.
[62] J.H. Song, J.H. Kim, S. Park, et al., Signaling responses of osteoblast cells to hydroxyapatite: the activation of ERK and SOX9, J Bone Miner Metab 26 (2) (2008) 138–142, https://doi.org/10.1007/s00774-007-0804-6.
[63] J. Zhang, M.T. Dalbay, X. Luo, et al., Topography of calcium phosphate ceramics regulates primary cilia length and TGF receptor recruitment associated with osteogenesis, Acta Biomater. 57 (2017) 487–497, https://doi.org/10.1016/j.actbio.2017.04.004.
[64] B. Chen, T. Lin, X. Yang, et al., Low-magnitude, high-frequency vibration promotes the adhesion and the osteogenic differentiation of bone marrow-derived mesenchymal stem cells cultured on a hydroxyapatite-coated surface: the direct role of Wnt/catenin signaling pathway activation, Int. J. Mol. Med. 38 (5) (2016) 1531–1540, https://doi.org/10.3892/ijmm.2016.2757.
[65] Y.R.V. Shih, Y. Hwang, A. Phadke, et al., Calcium phosphate-bearing matrices induce osteogenic differentiation of stem cells through adenosine signaling, Proc. Natl. Acad. Sci. U. S. A. 111 (3) (2014) 990–995, https://doi.org/10.1073/pnas.1321717111.
[66] S. Ibrahimi, L. D'Andrea, D. Gastaldi, M.W. Rivolta, P. Vena, Machine Learning approaches for the design of biomechanically compatible bone tissue engineering scaffolds, Comput. Methods Appl. Mech. Eng. 423 (2024), https://doi.org/10.1016/j.cma.2024.116842.
[67] A. Logeshwaran, R. Elsen, S. Nayak, Artificial intelligence-based 3D printing strategies for bone scaffold fabrication and its application in preclinical and clinical investigations, ACS Biomater Sci Eng.American Chemical Society 10 (2) (2024) 677–696, https://doi.org/10.1021/acsbiomaterials.3c01368.
[68] O. Ntousi, M. Roumpi, P.K. Siogkas, et al., Advances in computational modeling of scaffolds for bone tissue engineering: a narrative review of the Current approaches and challenges, Biomechanics 5 (4) (2025) 76, https://doi.org/10.3390/biomechanics5040076.